West Flemish Pass
Exploration Drilling Program

Chapter 5 – Physical Environment

Prepared for:
Chevron Canada Limited

Prepared by:
Stantec Consulting Ltd.
141 Kelsey Drive
St. John's, NL A1B 0L2
Tel: (709) 576-1458
Fax: (709) 576-2126

File No: 121415690

Final Report

January 2020

Table of Contents

LIST OF TABLES

LIST OF FIGURES

5.0 EXISTING PHYSICAL ENVIRONMENT

5.1 Geology and Geomorphology

The geology of the eastern Newfoundland offshore area is complex and dynamic. The current bedrock and surficial characteristics of the region have been shaped by various processes and by natural and human factors (AMEC 2014). The eastern continental shelf, formed during the Late Triassic to Cretaceous periods during the breakup of Pangea and the opening of the Atlantic Ocean, is underlain by pre-rift basement rocks (Enachescu 2014a). The area includes a series of Mesozoic rift basins created by a combination of rifting and salt tectonics, which includes the Orphan, Flemish Pass, Jeanne d'Arc, and Carson basins (Enachescu 2014a). The following sections provide an overview of the geology and geomorphology of the Project Area and surrounding areas.

5.1.1 Bedrock Geology

The Project Area (Figure 5-1) is located in the Flemish Pass Basin, which is approximately 14,000 km² (Enachescu 2012a). On the margin of the eastern continental shelf, the Flemish Pass Basin is saddle-shaped and occurs in a north-south orientation between the Grand Banks and the Flemish Cap (Cameron et al. 2014). The Flemish Pass Basin area is bound by the Dover Fault and Charlie-Gibbs Fracture Zone to the north, the Continent-Ocean Boundary to the east and south, and the Murre Fault and Mercury Fault to the west (Figure 5-2) (Edwards et al. 2003; Enachescu and Fagan 2004, Enachescu 2011); the Cumberland Belt Transfer Fault Zone overlaps the northern portion of the Flemish Pass Basin (Figure 5-2) (Enachescu and Fagan 2004). Located in 390-1,200 m of water (Enachescu 2014a), the Flemish Pass Basin is part of the North Atlantic Mesozoic rift network and is comprised primarily of Mesozoic rock overlying pre-rift, Appalachian basement rock of Avalon terrane (Fader et al. 1989; Cameron et al. 2014). Older Precambrian and Paleozoic rocks are found nearer to shore (Fader et al. 1989). Other basins in the area include the Orphan Basin and the Jeanne d'Arc Basin (Enachescu 2014b).

Before the Mesozoic rifting, this area was part of a broad Paleozoic sedimentary platform within the Avalon terrane of the Appalachian orogenic system (Williams et al. 1999). Within the North Atlantic, there were several major continental rifting phases including:

- Tethys rift phase (Late Triassic to Early Jurassic)—the initial narrow, northeast-southwest rift expanded within the Tethys rift system, which extended from the Gulf of Mexico to the Barents Shelf and northern Europe (Enachescu 2006, 2011).
- North Atlantic rift phase (Late Jurassic to Early Cretaceous)—the rift basin enlarged and deepened after a long thermal subsidence stage and connected the Flemish Pass Basin to the Orphan Basin (Enachescu 2006, 2011).
- Labrador Sea-Greenland rift phase (Early Cretaceous to Eocene)—Extension and minor trans-tension continued (Enchescu 2006, 2011).

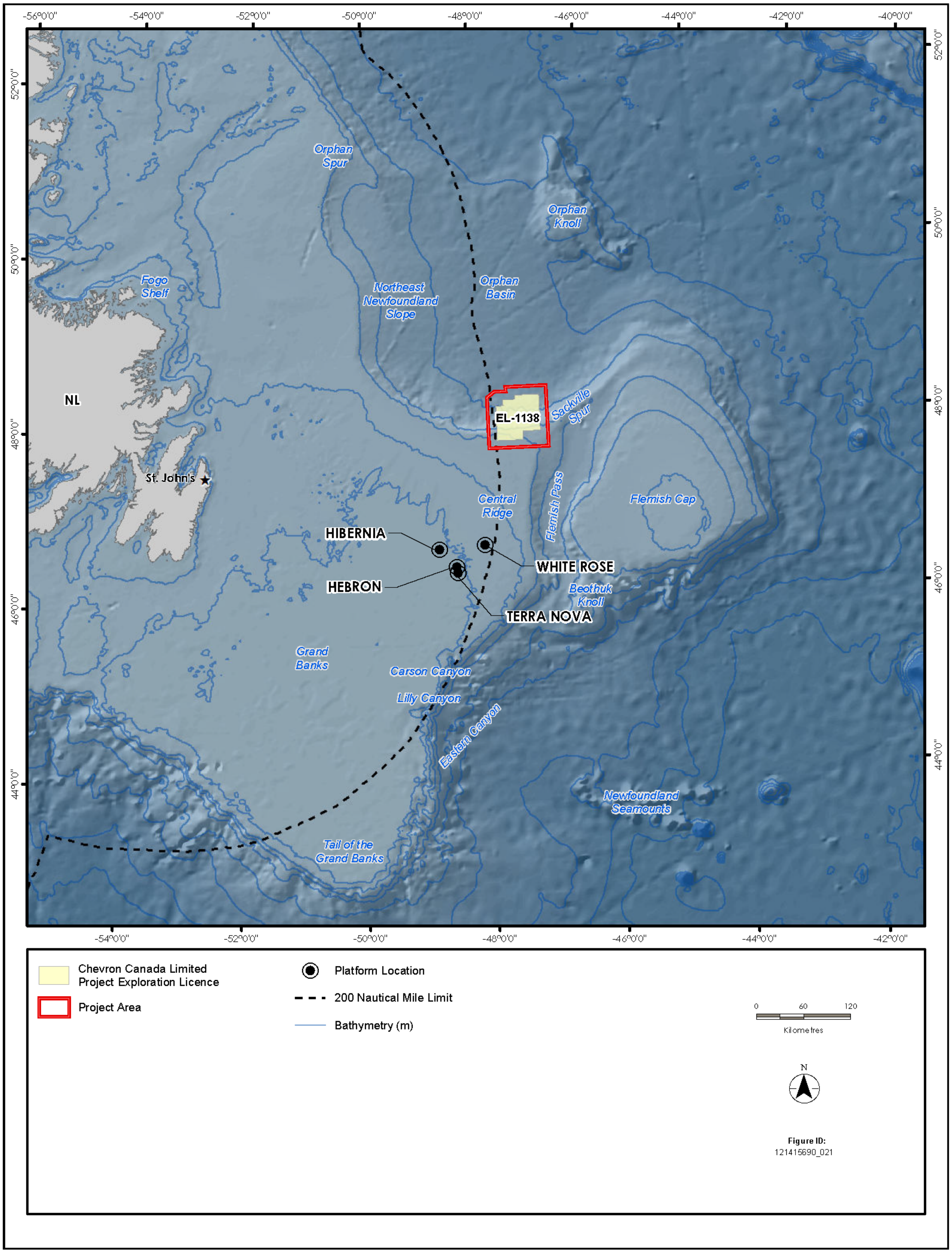

Figure 5-1 Geomorphic Features

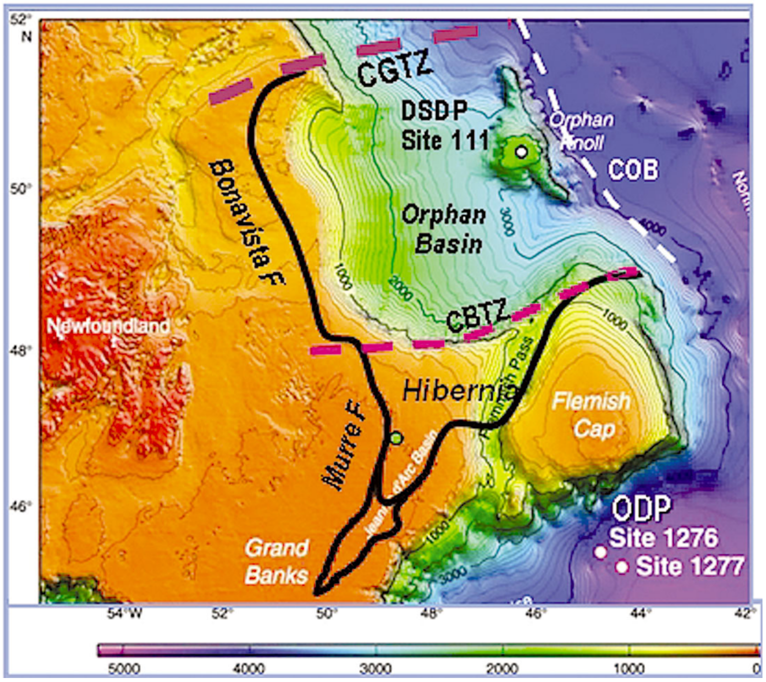

Source: Enachescu 2006

Note: CBZT = Cumberland Belt Transform Fault Zone; CGTZ = Charlie Gibbs Transform Fault Zone; COB = interpreted Continent-Ocean Boundary

Figure 5-2 Basin Boundaries and Fault Zones near the Flemish Pass Basin

These rifting events, combined with salt tectonics in the area, created a complex series of Mesozoic rift basins that are generally oriented northeast-southwest and are separated by basement highs along the central to outer shelf. The architecture of the Flemish Pass Basin is dominated by alternating ridges of basement block overlain by sediments and deep subbasins, which are predominantly oriented northeast-southwest or north-south (Enachescu 2006).

The Project Area overlaps two perched slope basins: the Flemish Pass Basin and Orphan Basin (Figure 5-3) (Fader et al. 1989). Geophysical evidence suggests that the Flemish Pass Basin is in contact with the East Orphan Basin, both of which had similar geologic histories in the Late Jurassic-Early Cretaceous (Enachescu et al. 2005). The primary reservoirs are located within the shallow marine and fluvial shale and sandstone that were deposited during the Late Jurassic and Early Cretaceous. The most substantial source rock in the Flemish Pass Basin is the Egret member of the Rankin Formation (Enachescu 2014a). Deposited in the Late Jurassic, Egret source rock is the primary source of oil and gas discoveries in the Jeanne d'Arc Basin (G and G Exploration Consulting Ltd 2003) and has been identified in the Flemish Pass Basin.

There are two distinct sectors within the Flemish Pass Basin based on tectonics, structural setting, and composition of sedimentary fill: the Gabriel Subbasin and the Baccalieu Subbasin (Enachescu 2014a). The Gabriel Subbasin occurs at the southerly portion of the Flemish Pass Basin and is separated from the Jeanne d'Arc Basin to the west by the north-south oriented Central Ridge. Sea depth is greater at the northern end of the Gabriel Subbasin, becoming shallower towards the south. While the Late Cretaceous sedimentary sequence is thin or absent due to erosion, the Early Cretaceous sequence in the Gabriel Subbasin is thick and contains promising reservoirs (Enachescu 2014a, 2014b, 2012b). The Baccalieu Subbasin is at the northern portion of the Flemish Pass Basin. At the northern margin, the water depth reaches 1,500 m and the Baccalieu Subbasin joins with the East Orphan Basin structures (Enachescu 2014a). The Baccalieu Subbasin overlaps the Sackville Spur, an elongated sediment drift. Separated from the eastern Flemish Cap by a tectonic line, seismic data from within the Baccalieu Subbasin indicate the presence of a Late Jurassic “hot shale” interval (Enachescu 2014a).

5.1.2 Geomorphology and Surficial Geology

The geomorphology and surficial geology of the Project Area and surrounding areas is a product of past glacial activity and modern oceanographic processes (Statoil 2017). The topography of the region is diverse, as characterized by depth, location, and physiography. While water depth in the Flemish Pass Basin is approximately 500 m to 1,500 m overall (Enachescu 2012a), water depth in the Project Area is approximately 300 m to 1,200 m (Enachescu 2014a). The major geomorphic features in or near the Project Area include the Sackville Spur, Central Ridge, and Flemish Cap (Table 5.1). Surface seabed features have been mapped for the Continental Margin of Eastern Canada (Figure 5-3).

Table 5.1 Geomorphic Features

Feature	Description
Sackville Spur	Prominent contourite drift formed at the northern end of the Flemish Pass Basin during the Neogene-Quaternary that has been incised by numerous canyons[1].
Central Ridge	Faulted intra-basinal high separating the Jeanne d’Arc Basin and the Flemish Pass Basin with water depth of approximately 500 m [2].
Flemish Cap	Large isolated continental basement high separated from the Grand Banks by the Flemish Pass Basin and the most easterly extension of the North American continental crust[3]. It is covered by a layer of sand several metres thick[4].
Flemish Pass Basin	Sedimentary basin that forms a terraced continuation of the East Orphan basin[5]. It consists of a central core of Hadrynian rocks, including granodiorites, granites, dacites, and an onlapping sequence of Mesozoic to Cenozoic aged sediments[6].
Orphan Knoll	Topographic high that rises 1,000 m above the Orphan Basin to the west, 1,600 m above the Orphan Basin to the south, and drops to 2,200 m to the Labrador Sea Abyssal Plain to the east. The knoll is oriented north-northwest-south-southeast and is approximately 75 km wide and 190 km long[7]
East Orphan Basin	Mesozoic basin in contact with the Flemish Pass Basin at its northern edge. Depths range from 1,500-3,500 m [8].
Bonavista Platform	Located between the shore and the Project Area. Seabed features in the area include iceberg scouring and to a lesser extent, seabed depressions of unknown origin[9].
Sources: 1 Kennard et al. 1990; 2 Enachescu 2011; 3 King et al. 1985; 4 Weitzman et al. 2014; 5 Lowe et al. 2011; 6 King et al. 1986; 7 Ruffman 2011; 8 Enachescu 2014a; 9 Cameron and Best 1985, in Statoil 2017	

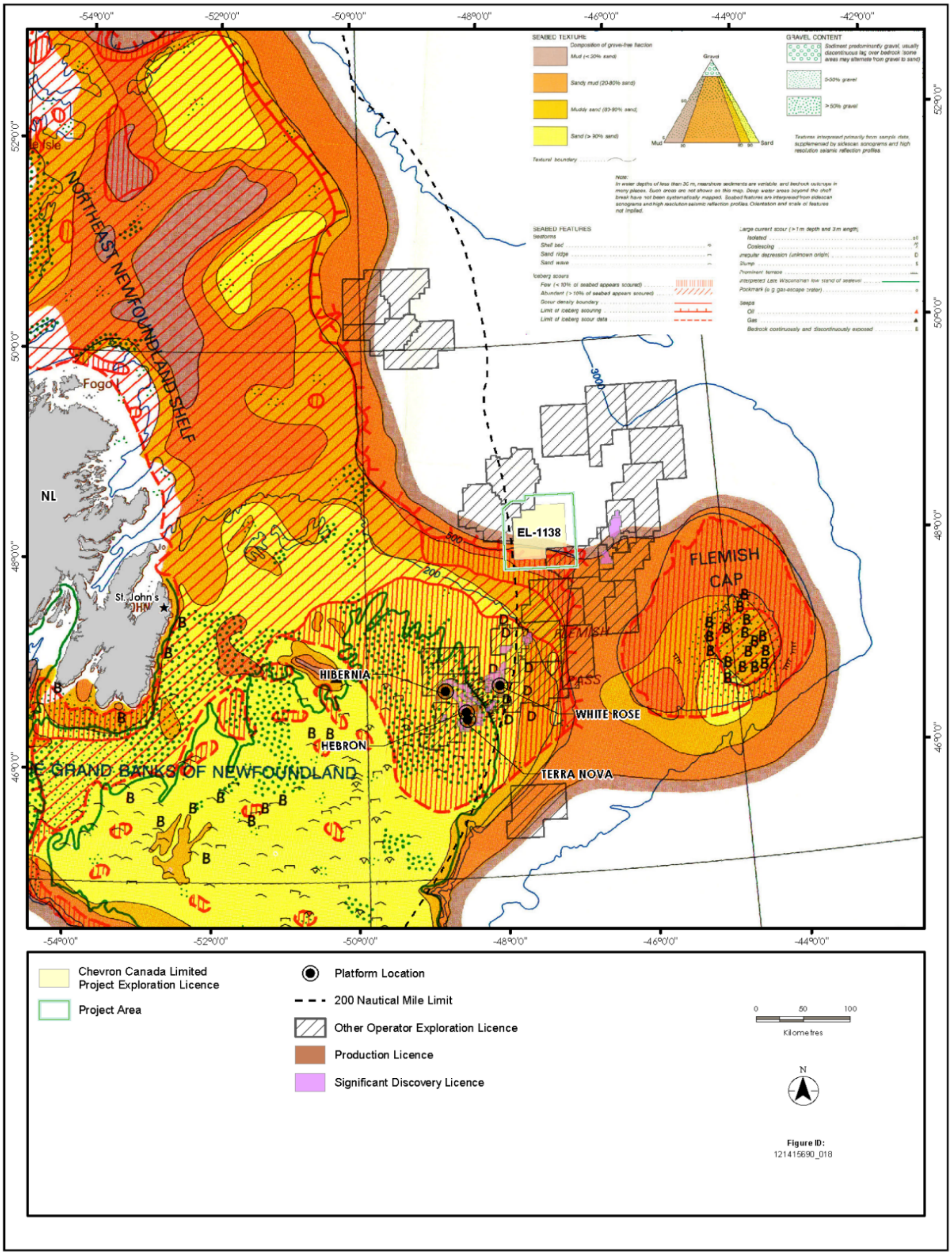

Source: Cameron and Best 1985

Figure 5-3 Eastern Newfoundland Seabed Features

The surficial geology of the region is highly variable. Almost the entire upper continental slope off Atlantic Canada is underlain by glacial till and some places, the till is buried up to tens of metres beneath younger proglacial and Holocene sediment (Edinger et al. 2011). Many till samples on the continental shelf and upper slope are composed of sand or mud that was derived from the reworking of Pleistocene or Late Tertiary sediments but include a small proportion of bedrock ranging from pebbles to boulders (Edinger et al. 2011). Deeper basins, such as the Flemish Pass Basin, are generally silt or clay-filled (Statoil 2017). The primary reservoirs within the Flemish Pass Basin occur in shallow marine and fluvial shale and sandstone that was deposited during the late Jurassic and Early Cretaceous periods of the Mesozoic Era (Statoil 2017). The seabed on the slope of the Flemish Pass Basin generally consists of Holocene silty clay (Statoil. 2017). Winnowed sands are present on parts of the Flemish Pass Basin floor (Murillo et al. 2016). Coarser-grained sediments are found through the center and western side of the Flemish Pass Basin while finer-grained sediments are concentrated predominately on the eastern side of the Pass, including the terrace (Marshall et al. 2014). There is also potential for gravel and ice-rafted cobbles and/or boulders on the seafloor and in the shallow subsurface (Fugro 2017, in Statoil 2017).

In general, eroded Quaternary sediments and authigenic carbonates [carbonate mineral precipitated inorganically *in situ*, whether at the water-sediment interface or within sediment pore waters (Schrag et al. 2013)] are thought to be more common than eroded Tertiary bedrock along the shelf break and upper slope of NL (Piper et al. 2005; Edinger et al. 2011). Quaternary sediments in the northern portion of the Project Area include: turbidite sands and muds and proglacial muds derived from the Grand Banks; ice-rafted and proglacial plume deposits transported southward in the Labrador Current; and debris-flow deposits (Equinor 2018). These sediments have been described as follows (Piper and Cameron 2005, in Statoil 2017). In the northern Flemish Pass Basin deposits up to 120 m thick have been recognized and are interpreted as debris-flow deposits thought to be derived from sediment failures that have left scarps both on the southeast side of Sackville Spur and on the north-west side of the Flemish Cap. Sediments recovered from this area are generally lean silt to lean clay and are considered to be normally consolidated. The western slopes of the Flemish Pass Basin are comprised mainly of muds with some coarse-grained ice-rafted detritus. Interbedded sandy turbidites are most abundant 2 to 3.5 m below sea floor. Successions of silty muds with ice-rafted detritus, thin sand, and mud turbidites overlie thick bedded sand turbidites on the floor of the central part of the Flemish Pass Basin. The eastern slopes of the Flemish Pass Basin have sediment consisting primarily of mud with sparse ice-rafted detritus. On the Sackville Spur, 8 m of sandy gravelly mud has been locally observed overlying 4.5 m of grey mud, and then a further 12 m of gravelly sandy mud.

5.2 Seismicity

The Eastern NL SEA (AMEC 2014) describes Eastern Canada as stable area of relatively low-level seismic activity. There are approximately 450 earthquakes that occur annually in Eastern Canada, with most between magnitude two and three (AMEC 2014). The probability of earthquake occurrences in Canada are illustrated in the Seismicity Hazard Map of Canada (Figure 5-4); the Project Area and RAA are in an area of low seismic hazard (NRCan 2018).

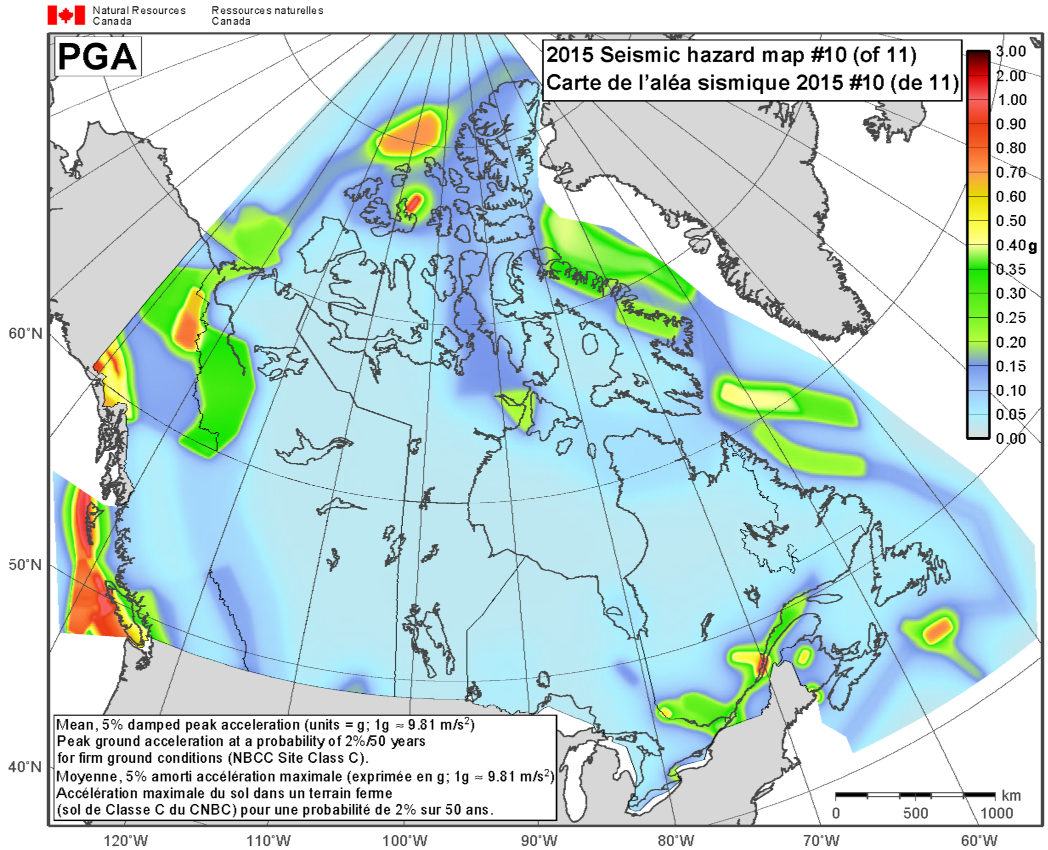

Source: NRCan 2018
Note: Peak ground acceleration at a probability of 2%/50 years for firm ground conditions (NBCC Site Class C). Peak acceleration is contoured in g.

Figure 5-4 Seismicity Hazard Map of Canada – Peak Ground Acceleration

Between 1985 and 2019, 55 earthquakes have occurred in the RAA (Figure 5-5) (NRCan 2019). Of these, 44 had magnitudes of two to four, and 11 of these had magnitudes of four to 4.7 (NRCan 2019). No earthquakes have occurred within or bordering on the Project Area. Most of the earthquake epicentres (Figure 5-5) are to the northwest and southwest of the Project Area.

5.3 Bathymetry

EL 1138 is located just west of northern extent of the Flemish Pass, skirting the eastern border of the Grand Banks and northern bank of the Sackville Spur as they quickly drop away into the deeper waters of the Orphan Basin (Figure 5-6). The Sackville Spur, immediately adjacent to the eastern boundary of EL 1138, has a water depth to 1,000 m. The Orphan Basin (immediately north of EL 1138) reaches depths of 1,200 to 3,500 m (AMEC 2014). Depths at the southern border of EL 1138, which lie in the shallower waters of the bank, range from 400 to 600 m. The seafloor then drops away at a largely uniform gradient to 1,700 m, whereupon a series of pronounced submarine gullies are visible (noticeably in the 2,000 m isobath). These appear to largely dissipate upon reaching the maximum depth of approximately 2,300 m in the northeastern most corner.

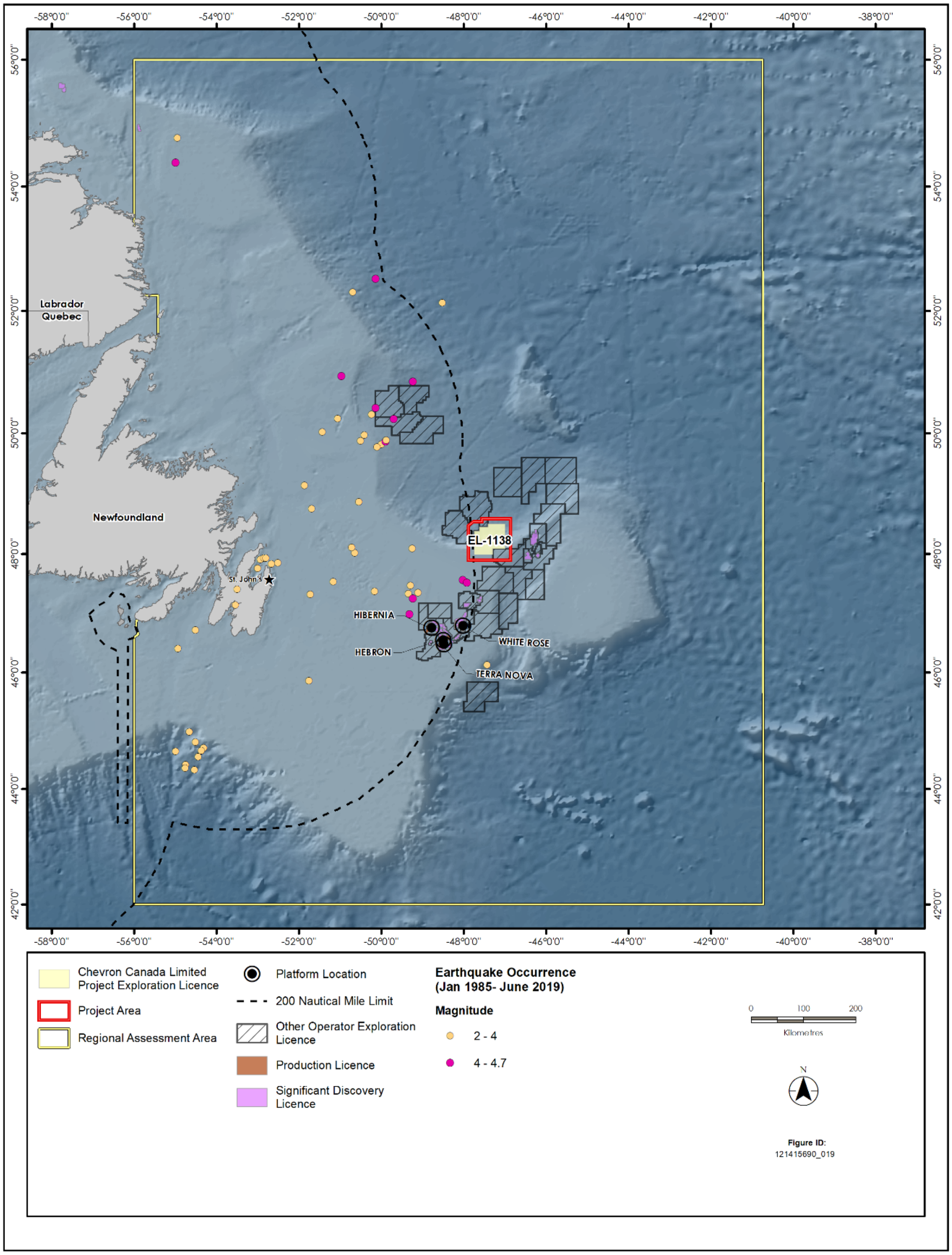

Source: NRCan 2019

Figure 5-5 Earthquake Epicentres (1985 to 2019) in the RAA

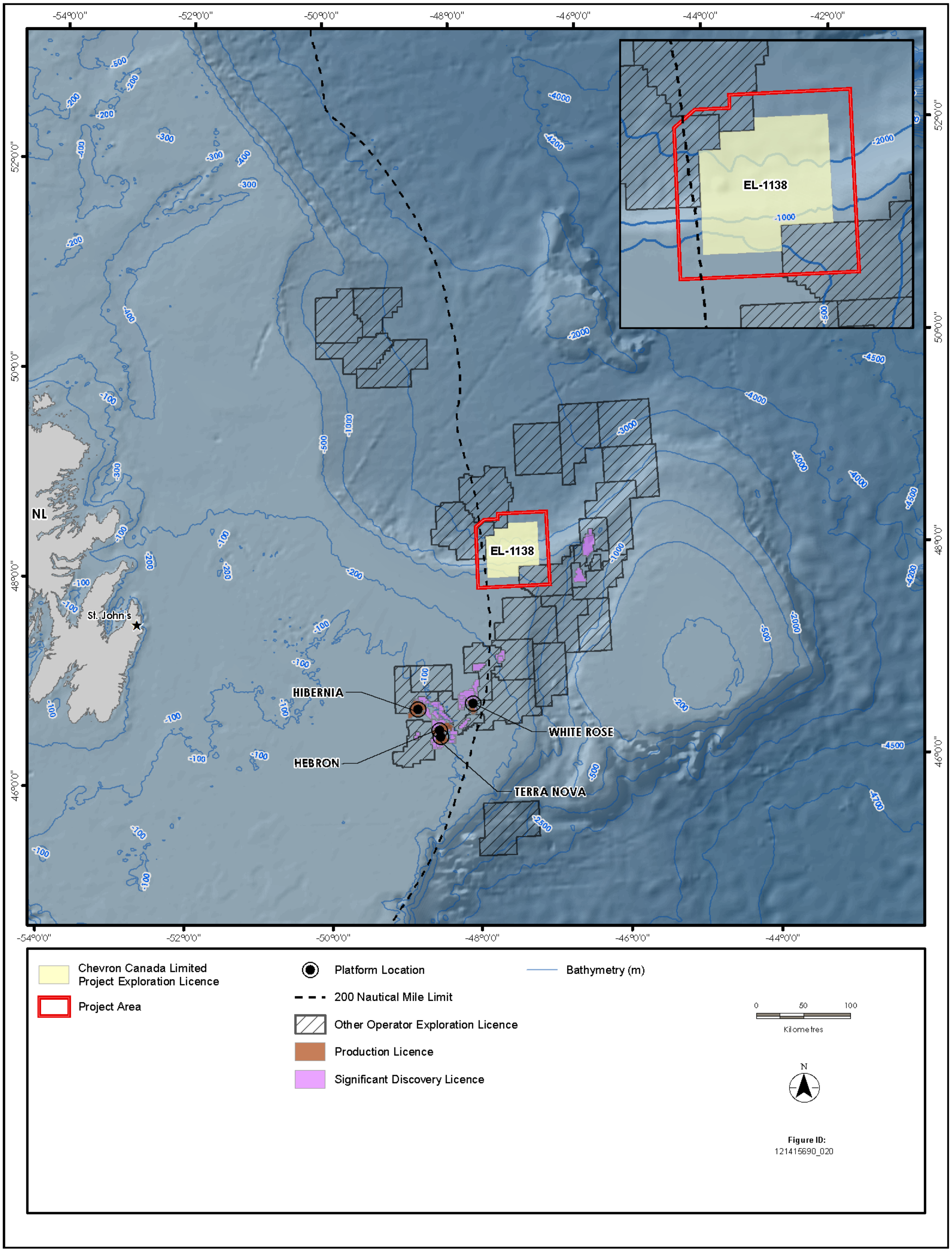

Figure 5-6 Bathymetry of Project Area

5.4 Climatology

The Grand Banks region area experiences weather conditions typical of a marine environment with the surrounding waters having a moderating effect on temperature. In general, marine climates experience cooler summers and milder winters than continental climates and have a much smaller annual temperature range. Furthermore, a marine climate tends to be humid, resulting in reduced visibility, low cloud heights, and substantial amounts of precipitation.

The climate of the area is dynamic, being largely governed by the passage of high and low-pressure circulation systems. These circulation systems are embedded in, and steered by, the prevailing westerly flow that typifies the upper levels of the atmosphere in the mid-latitudes, which arises because of the normal tropical to polar temperature gradient. The mean strength of the westerly flow is a function of the intensity of this gradient and is considerably stronger in the winter months than during the summer months, due to an increase in the south to north temperature gradient. Meteorological convention defines seasons by quarters (e.g., winter is December, January, February).

At any given time, the upper level flow is a wave-like pattern of large and small amplitude ridges and troughs. These ridges and troughs tend to act as a steering mechanism for surface features and therefore their positions in the upper atmosphere determine the weather at the earth's surface. Upper ridges tend to support areas of high pressure at the surface, while upper troughs lend support to low-pressure developments. The amplitude of the upper flow pattern tends to be higher in winter than summer, which is conductive to the development of more intense storm systems.

During the winter months, an upper level trough tends to lie over Central Canada and an upper ridge over the North Atlantic resulting in three main storm tracks affecting the region: one from the Great Lakes Basin, one from Cape Hatteras, North Carolina and one from the Gulf of Mexico. These storm tracks, on average, bring eight low-pressure systems per month over the area. The intensity of these systems ranges from relatively weak features to major winter storms. There exists a poleward shift of the jet stream, and consequently storm tracks, at a rate of 0.17 to 0.19 degrees per decade in the northern hemisphere. This shift has been related to an increase in the equator-to-pole temperature gradient. There has been a decrease in mid-latitude cyclone frequency and an increase in high-latitude cyclone frequency. In addition, storm intensity has increased in both the high- and mid-latitudes.

In the case where the upper level long wave trough lies well west of the region, the main storm track will lie through the Gulf of St. Lawrence or Newfoundland. Under this regime, an east to southeast flow ahead of a warm front associated with a low will give way to winds from the south in the warm sector of the system. Typically, the periods of southerly winds and mild conditions will be of relatively long duration, and in general, the incidence of extended storm conditions is likely to be relatively infrequent. Strong frictional effects in the stable flow from the south results in a marked shear in the surface boundary layer and relatively lower winds at the sea surface. Consequently, local wind wave development tends to be inhibited under such conditions. Precipitation types are more likely to be in the form of rain or drizzle, with relatively infrequent periods of continuous snow, although periods of snow showers prevail in the unstable air in the wake of cold fronts associated with the lows. Visibility will be reduced at times in frontal and advection fogs, in snow, and in snow shower activity.

At other times, with the upper long wave trough situated further to the east, the main storm track may lie through or to the east of the Grand Banks. With the lows passing closer to the site and a higher potential for storm development, the incidence of strong gale and storm conditions is greater. Longer bouts of cold, west to northwest winds behind cold fronts occur more frequently, and because the flow is colder than the surface water temperatures, the surface layer is unstable. The shear in the boundary layer is lower, resulting in relatively higher wind speeds near the surface, and consequently relatively higher sea state conditions. With cold air and sea surface temperatures coupled with high winds, the potential for freezing spray will occur quite frequently. In this synoptic situation, a greater incidence of precipitation in the form of snow is likely to occur. Freezing precipitation, either as rain or drizzle, occurs rather infrequently on the Grand Banks. Visibility will be reduced in frontal and advection fogs, and relatively more frequently by snow.

Frequently, intense low-pressure systems become “captured” and slow down or stall off the coast of NL. This may result in an extended period of little change in conditions that may range, depending on the position, overall intensity and size of the system, from the relatively benign to heavy weather conditions.

By summer, the main storm tracks have moved further north than in winter. Low-pressure systems are less frequent and much weaker. With increasing solar radiation during spring, there is a general warming of the atmosphere that is relatively greater at higher latitudes. This decreases the north-south temperature contrast, lowers the kinetic energy of the westerly flow aloft and decreases the potential energy available for storm development. Concurrently, there is a northward shift of the main band of westerly winds at upper levels and a marked development of the Bermuda-Azores sub-tropical surface through the entire troposphere. The main track of the weaker low-pressure systems typically lies through the Labrador region and tends to be oriented from the west-southwest to the east-northeast. With low-pressure systems normally passing to the north of the region in combination with the northwest sector of the sub-tropical high to the south, the prevailing flow across the Grand Banks is from the southwest during the summer season. Wind speed is lower during the summer and the incidence of gale or storm force winds relatively infrequent. There is also a corresponding decrease in significant wave heights. The prevailing southwesterly flow during the late spring and early summer tends to be moist and it is relatively warmer than the underlying surface waters on the Grand Banks.

Rapidly deepening storms are a problem south of Newfoundland in the vicinity of the warm water of the Gulf Stream. Sometimes these explosively deepening oceanic cyclones develop into a “weather bomb”, defined as a storm that undergoes central pressure falls greater than 24 mb over 24 hours with hurricane force winds near the centre. The outbreak of convective clouds to the north and east of the centre during the explosive stage, and the presence of a clear area near the center in its mature stage are typical of weather bombs. After development, these systems will either move across Newfoundland or to the east of Newfoundland producing gale to storm force winds from the southwest to south over the Grand Banks.

In addition to extratropical cyclones, tropical cyclones often retain their tropical characteristics as they enter the RAA. Tropical cyclones account for the strongest sustained surface winds observed anywhere on earth. The hurricane season in the North Atlantic basin normally extends from June through November, although tropical storm systems occasionally occur outside this period. Once formed, a tropical storm or hurricane will maintain its energy as long as a sufficient supply of warm, moist air is available. Tropical storms and hurricanes obtain their energy from the latent heat of vaporization that is released during the condensation process. These systems typically move east to west over the warm water of the tropics; however, some of these systems turn northward and make their way towards Newfoundland. Since the capacity of the air to hold water vapor is dependent on temperature, as the hurricanes move northward over the colder ocean waters, they begin to lose their tropical characteristics. By the time these weakening cyclones reach Newfoundland, they are usually embedded into a mid-latitude low and their tropical characteristics are usually lost.

A substantial number of tropical cyclones, which move into the mid-latitudes will undergo transition into extratropical cyclones. On average, 46% of tropical cyclones, which formed in the Atlantic transform into extratropical cyclones. During this transformation, the system loses tropical characteristics and becomes more extratropical in nature. These systems frequently produce large waves, gale to hurricane force winds and intense rainfall. The likelihood that a tropical cyclone will undergo transition increases toward the second half of the tropical season, with October having the highest probability of transition. In the Atlantic, extratropical transition occurs at lower altitudes in the early and late hurricane season and at higher latitudes during the peak of the season.

5.4.1 Wind Speed and Direction

The Meteorological Service of Canada 50 North Atlantic Wave Hindcast (MSC50) North Atlantic wind and wave climatology database is used to analyze wind climatology in this area. The database is compiled by Oceanweather Inc under contract to Environment Canada. The MSC50 database consists of continuous wind and wave hindcast data in 1-hour time steps from January 1954 to December 2015, on a 0.1° latitude by 0.1° longitude grid. Winds from the MSC50 data are 1-hour averages of the effective neutral wind at a height of 10 m.

Climatology is typically described using 30-year periods of data, which is considered short enough to reduce the effects of long-term climate change on the statistics, yet long enough to reduce the impact of anomalous events. Therefore, a 30-year subset of the MSC50 data from 1986 to 2015 is used for the analysis. Grid point 13741 (48.2°N and 47.3°W) is chosen to represent conditions within the area of interest.

The Project Area experiences predominately southwest to northwest flow throughout the year (Table 5.2). West to northwest winds, which are prevalent during the winter months, begin to shift counter-clockwise during spring months, resulting in a predominant southwest wind by the summer months. As autumn approaches, the tropical-to-polar temperature gradient strengthens and the winds shift slightly, becoming predominately westerly again by late fall and into winter.

Table 5.2 Monthly and Annual Percentage Frequency of Wind Direction at MSC50 Gridpoint 13741 (1954 to 2015)

Month	Direction							
	NE	E	SE	S	SW	W	NW	N
January	3.2	3.5	7.0	11.6	20.0	33.3	16.9	4.6
February	3.7	5.3	8.6	11.5	18.5	29.4	16.2	6.8
March	6.5	6.8	7.5	11.6	16.7	23.4	17.4	10.0
April	7.4	9.1	9.3	11.8	17.7	18.0	15.8	11.1
May	8.3	7.6	8.1	15.7	19.5	16.2	13.9	10.8
June	6.4	7.1	8.0	16.2	27.4	15.4	11.8	7.7
July	2.9	3.9	6.8	18.9	36.2	17.8	10.4	7.0
August	5.6	5.1	6.5	16.7	31.3	17.3	10.4	7.0
September	4.5	4.4	6.1	15.0	24.1	20.6	16.3	9.0
October	6.1	5.5	6.7	12.2	18.1	22.5	19.2	9.7
November	3.9	4.3	8.2	12.7	18.9	24.3	21.2	6.5
December	4.9	6.0	7.2	10.9	16.8	27.6	19.2	7.4
Annual	5.3	5.7	7.5	13.8	22.1	22.1	15.6	7.9

Low-pressure systems crossing the area are more intense during the winter months. As a result, mean wind speeds tend to peak during this season. As shown in Table 5.3, mean wind speed sets peak during the month of January, reaching a magnitude of 12.2 m/s, and maximum wind speed is also observed in the same month with a speed of 33.9 m/s.

In addition, remnants of tropical systems pass near Newfoundland between spring and late fall. Therefore, while mean wind speeds tend to peak during the winter months, maximum wind speeds may occur at any time during the year. Monthly maximum wind speed by direction is given in Table 5.4.

Table 5.3 Mean, Maximum, and Standard Deviation of Wind Speed (m/s) Statistics at MSC50 Gridpoint 13741 (1954 to 2015)

Month	Mean	Maximum	Standard Deviation
January	12.2	33.9	4.5
February	11.6	30.3	4.6
March	10.6	29.4	4.3
April	8.7	26.8	4.0
May	7,4	21.3	3.5
June	6.9	20.1	3.3
July	6.4	18.5	3.0
August	6.6	25.9	3.1
September	8.0	28.4	3.7
October	9.3	30.4	3.9
November	10.5	26.6	4.3
December	11.3	29.8	4.5

Table 5.4 Monthly Maximum Wind Speed (m/s) by Direction at MSC50 Gridpoint 13741 (1954 to 2015)

Month	Direction							
	NE	E	SE	S	SW	W	NW	N
January	19.7	21.5	25.0	24.2	27.2	33.9	28.7	24.7
February	24.5	22.4	26.2	29.8	30.3	30.0	26.6	22.9
March	18.4	20.9	22.5	22.8	24.5	29.4	27.6	21.1
April	19.1	20.4	21.0	22.1	21.5	23.6	25.2	26.8
May	21.1	16.9	16.2	18.4	21.1	19.5	21.3	18.9
June	14.2	15.4	20.1	16.8	18.3	18.6	18.5	15.7
July	14.4	14.5	16.6	18.5	17.4	16.6	15.6	16.0
August	21.8	19.1	25.9	23.4	20.0	23.0	19.8	21.4
September	16.6	17.2	28.4	27.1	27.6	25.2	22.5	18.8
October	18.4	20.3	23.7	30.4	28.2	26.3	27.1	26.0
November	21.4	22.8	23.3	21.4	26.6	26.6	25.8	25.9
December	21.1	21.9	24.5	24.3	26.2	28.7	29.8	22.7

In addition to mid-latitude low-pressure systems crossing the Grand Banks, tropical cyclones often move northward out of the influence of the warm waters of the Gulf Stream, passing near the Island of Newfoundland. Once the cyclones move over colder waters, they lose their source of latent heat energy and often begin to transform into a fast-moving and rapidly developing extratropical cyclone producing large waves and sometimes hurricane force winds.

A wind rose of the annual wind speed is presented in Figure 5-7 and the associated histogram of the wind speed frequency in Figure 5-8. Percentage frequency of wind direction by month is presented in Table 5.2. Wind speeds are much lower in the summer than in the winter. The percentage exceedance of wind speeds is presented in Figure 5-9.

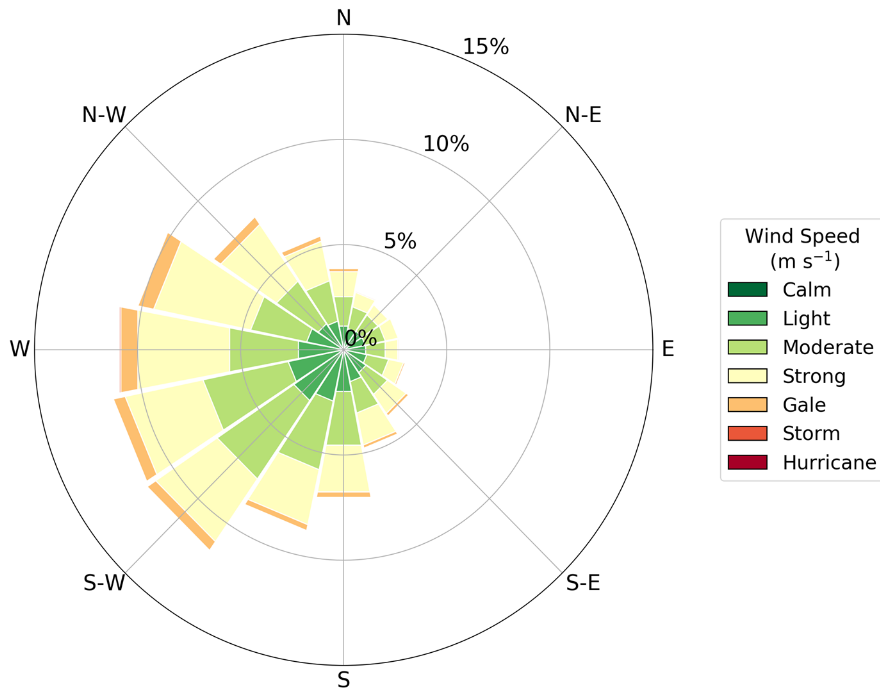

Figure 5-7 Annual Wind Rose for MSC50 Grid Point 13741 for 1954 to 2015

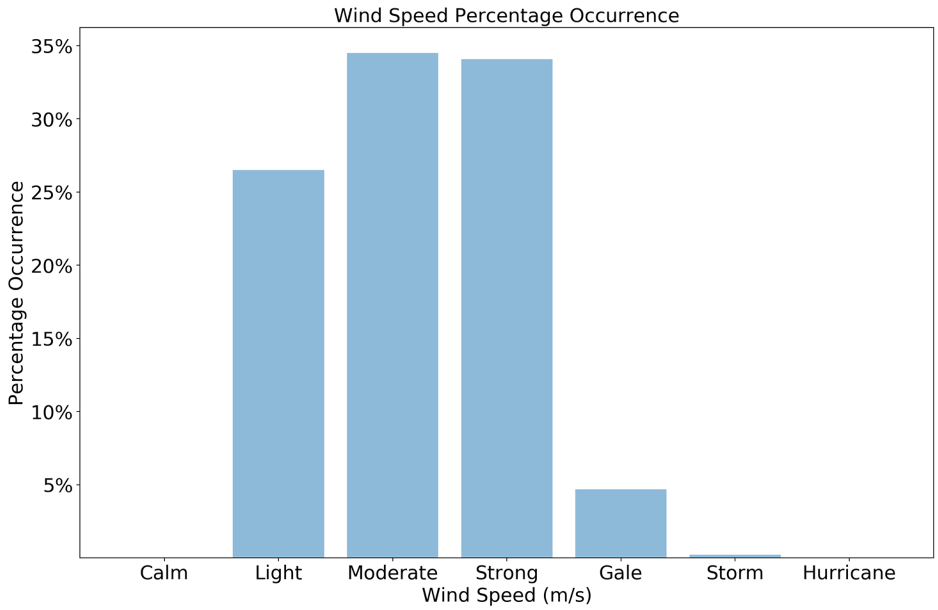

Figure 5-8 Annual Percentage Frequency of Wind Speeds for Grid Point 13741 for 1954 to 2015

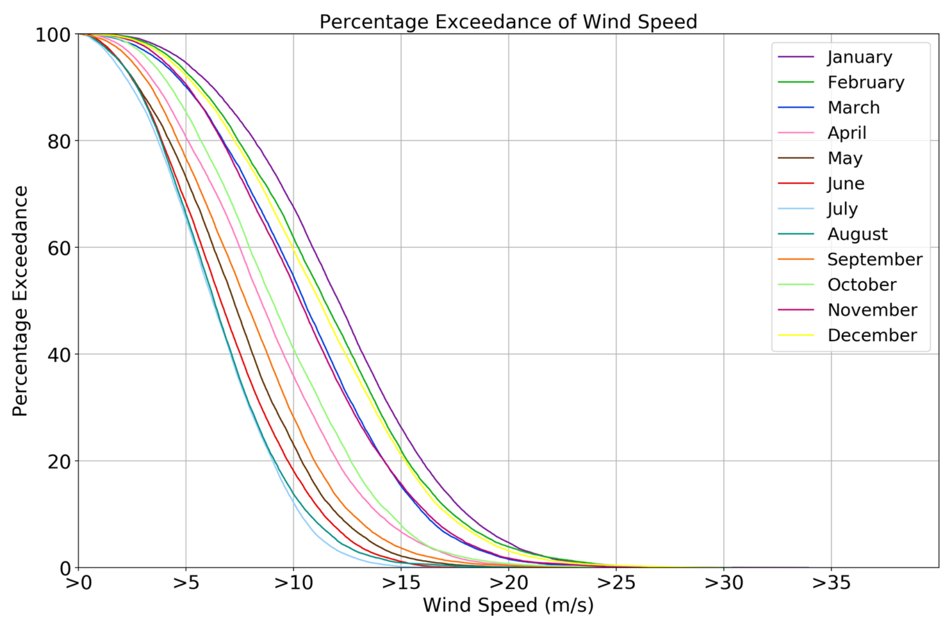

Figure 5-9 Percentage Exceedance of Wind Speed at Grid Point 13741 for 1954 to 2015

5.4.2 Air and Sea Temperature

Air and sea temperatures for the area are extracted from the International Comprehensive Ocean-Atmosphere Data Set (ICOADS). The data set consists of global marine surface observations from ships, drilling rigs, and buoys. A subset of the ICOADS data set for the area from 47°N to 49°N and 48°W to 46°W covering the period from January 1986 to December 2015 is used for the analysis of air and sea temperature.

The moderating influence of the ocean serves to limit both the diurnal and the annual temperature variation on the Grand Banks. Diurnal temperature variations due to the day/night cycles are small. Short- Short-term, random temperature changes are due mainly to a change of air mass following a warm or cold frontal passage. In general, air mass temperature contrasts across frontal zones are greater during the winter than during the summer season.

A monthly plot of air temperature versus sea surface temperature is presented in Figure 5-10. Air and sea surface temperature statistics are presented in Tables 5.5 and 5.6. The atmosphere is coldest in the month of February with a mean monthly air temperature of -0.5°C, and warmest in August with a mean monthly air temperature of 13.1°C. Similarly, sea surface temperature is warmest in August with a mean monthly temperature of 12.4°C and coldest in March with mean monthly temperature of 2.1°C.

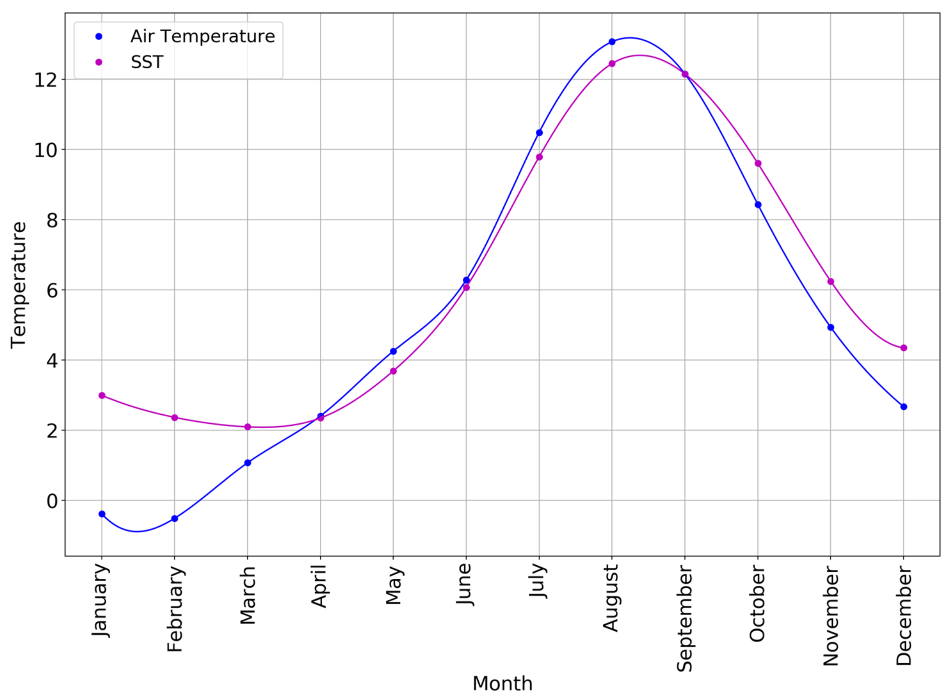

Figure 5-10 Monthly Mean Air and Sea Temperature (°C) from the ICOADS Data Set (1986 to 2015)

Table 5.5 ICOADS Air Temperature (°C) Statistics from the ICOADS Data Set (1986 to 2015)

Month	Mean	Maximum	Minimum	Standard Deviation	Mean Daily Maximum	Mean Daily Minimum
January	-0.4	12.0	-11.4	3.7	1.8	-0.5
February	-0.5	13.8	-13.0	3.5	1.2	-1.0
March	1.1	14.0	-10.0	3.3	2.5	0.3
April	2.4	15.0	-6.0	2.4	3.7	2.0
May	4.3	18.0	-3.0	2.1	5.5	3.7
June	6.3	17.0	0.1	2.8	7.7	6.1
July	10.5	23.4	1.4	2.5	11.4	10.0
August	13.1	22.0	4.1	2.1	14.0	12.8
September	12.2	22.0	4.8	2.3	13.0	11.6
October	8.4	20.0	1.2	2.4	9.5	8.3
November	4.9	19.7	-4.5	2.9	6.3	4.7
December	2.7	17.0	-7.0	3.1	3.9	2.3

Table 5.6 ICOADS Sea Surface Temperature (°C) Statistics from the ICOADS Data Set (1986 to 2015)

Month	Mean	Maximum	Minimum	Standard Deviation
January	3.0	14.0	-2.1	1.9
February	2.4	12.4	-2.1	1.7
March	2.1	14.0	-2.0	1.8
April	2.3	14.4	-2.0	1.8
May	3.7	16.0	-1.5	1.8
June	6.1	18.0	-1.0	1.8
July	9.8	22.0	1.0	2.5
August	12.4	18.5	5.5	2.3
September	12.2	20.0	3.0	2.0
October	9.6	21.0	1.0	2.4
November	6.2	18.0	0.1	1.9
December	4.3	16.0	-2.3	1.9

The mean sea surface temperature is cooler than the mean air temperature from April to September, with the greatest difference occurring in the months of July and August. From September to April, sea surface temperatures are warmer than the mean air temperature. The colder sea surface temperatures from April to September have a cooling effect on the atmosphere, while relatively warmer sea surface temperatures from September to April tend to warm the overlying atmosphere.

Monthly mean daily maximum and minimum temperature statistics are also presented. Mean temperatures for each month are the mean of all temperatures recorded at the site during that month. The maximum and minimum temperatures are the highest and lowest temperatures, respectively, recorded during the month over the entire data set. The mean daily maximum is the average of all maximum temperatures recorded during the specified month, while the mean daily minimum is the average of all minimum temperatures recorded during the specified month.

5.4.3 Precipitation

The frequency of precipitation type for the Project Area is calculated using data from the ICOADS data set covering the same region and time period as for the analysis of air and sea surface temperature. Precipitation can come in three forms and are classified as liquid, freezing or frozen:

- Liquid Precipitation
  - Drizzle
  - Rain
- Freezing Precipitation
  - Freezing Drizzle
  - Freezing Rain
- Frozen Precipitation
  - Snow
  - Snow Pellets
  - Snow Grains
  - Ice Pellets
  - Hail
  - Ice Crystals

The migratory high and low-pressure systems transiting the temperature middle latitude of the Northern Hemisphere cause a variety of precipitation types in their paths. Each occurrence of one precipitation type is counted as one event. Precipitation statistics may be low due to a fair weather bias. That is, ships tend to either avoid regions of inclement weather, or simply do not report during these events.

The frequency of precipitation type shows that annually, precipitation occurs 21.3% of the time (Table 5.7). Winter has the highest frequency of precipitation with 32.4% of the observations. Snow accounts for most precipitation during the winter months, accounting for 17.3% of the occurrences of winter precipitation. Summer has the lowest frequency of precipitation with a total frequency of occurrence of only 14.4%.

Table 5.7 Percentage Frequency (%) Distribution of Precipitation for ICOADS Data Set from the ICOADS Data Set (1986 to 2015)

Month	Rain / Drizzle	Freezing Rain / Drizzle	Rain/Snow Mixed	Snow	Thunderstorm	Hail	Total
January	12.3	0.3	3.2	21.4	0.1	0.1	37.4
February	12.5	0.2	1.3	18.3	0.0	0.0	32.4
March	11.9	0.2	1.6	11.9	0.0	0.2	25.9
April	11.2	0.2	0.6	4.6	0.0	0.1	16.6
May	13.8	0.0	0.2	2.1	0.0	0.0	16.1
June	16.3	0.1	0.0	0.3	0.2	0.0	16.9
July	13.4	0.0	0.0	0.1	0.1	0.0	13.5
August	12.9	0.0	0.0	0.0	0.2	0.1	13.2
September	14.0	0.1	0.0	0.1	0.0	0.0	14.2
October	19.2	0.1	0.0	0.4	0.0	0.0	19.8
November	15.3	0.1	1.1	3.6	0.0	0.1	20.2
December	13.2	0.2	1.7	10.0	0.0	0.0	25.1
Winter	12.6	0.2	2.1	17.3	0.0	0.0	32.4
Spring	12.3	0.1	0.8	6.3	0.0	0.1	19.6
Summer	14.1	0.0	0.0	0.1	0.1	0.0	14.4
Autumn	16.1	0.1	0.4	1.4	0.0	0.0	18.0
All Years	13.6	0.1	0.9	6.6	0.0	0.0	21.3

Freezing precipitation occurs when rain or drizzle aloft enters negative air temperature near the surface and becomes super-cooled so that the droplets freeze upon impact with the surface. This situation typically arises ahead of a warm front extending from low-pressure systems passing west of the area. Since negative air temperature is required for freezing precipitation, statistics show that the frequency of freezing precipitation is slightly higher in winter than during spring and autumn. On a monthly basis, January has the highest frequency of freezing precipitation, approximately 0.3% of the time.

Thunderstorms occur relatively infrequently over the Project Area though they may occur in any month of the year. It is worth noting that hail only occurs in the presence of severe thunderstorms, yet in Table 5.7 the frequency of hail is higher than the frequency of thunderstorms during the months of March, April and November. This may be due to observer inexperience, classifying what should be ice pellets (formed through entirely different atmospheric processes) as hail or through coding error.

5.4.4 Fog and Visibility

Visibility is defined as the greatest distance at which objects of suitable dimensions can be seen and identified. Horizontal visibility may be reduced by the following phenomena, either alone or in combination as follows:

- Fog (visibility less than 1 km)
- Mist (visibility less than 10 km)
- Smoke
- Liquid Precipitation (e.g., drizzle)
- Freezing Precipitation (e.g., freezing rain)
- Frozen Precipitation (e.g., snow)
- Blowing Snow

Obstructions to visibility can occur in any month (Figure 5-11). Annually, 37.9% of the observations have visibility less than 10 km. During winter months, the main obstruction is snow; however, mist and fog may also reduce visibility at times. As spring approaches, the amount of visibility reduction attributed to snow decreases. As the air temperature increases, so does the occurrence of advection fog. Advection fog forms when warm moist air moves over cooler waters. By April, the sea surface temperature south of Newfoundland is cooler than the surrounding air. As warm moist air from the south moves over the colder sea surface, the air cools and its ability to hold moisture decreases. The air will continue to cool until it becomes saturated and the moisture condenses to form fog. The presence of advection fog increases from April through July. The month of July has the highest percentage of obstruction of visibility, most of which is in the form of advection fog, although frontal fog can also contribute to the reduction in visibility. Starting from August, the temperature difference between the air and the sea begins to decrease and by September the air temperature begins to fall below the sea surface temperature. As the air temperature drops, the occurrence of fog decreases. Reduction in visibility during autumn and winter is relatively low and is mainly attributed to the passage of low-pressure systems. Fog is the main cause of the reduced visibility in autumn, and snow is the main cause of reduced visibility in winter. October has the lowest occurrence of reduced visibility since the air temperature has, on average, decreased below the sea surface temperature and it is not yet cold enough for snow.

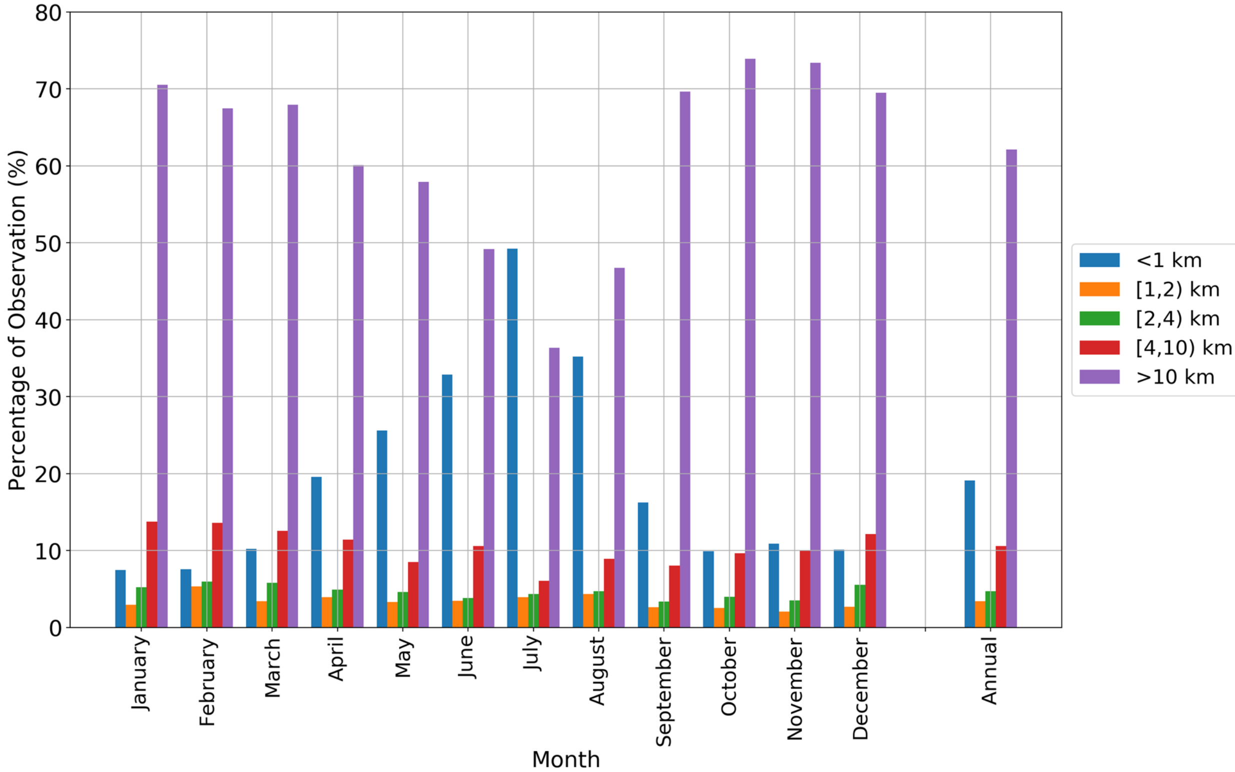

Figure 5-11 Monthly and Annual Percentage Occurrence of Visibility from the ICOADS Data Set (1986 to 2015)

Fog also occurs as relatively warm rain falls through cooler air beneath a frontal surface. Typically, the base of the cloud layer lowers as the air becomes saturated and condensation occurs. If the cloud base reaches the surface, frontal fog occurs. Most frequently, frontal fog occurs ahead of a warm front associated with a frontal disturbance. As the front moves through, clearing of the fog may occur but frequently, frontal fog gives way to advection fog in the warm sector of a low-pressure system. Typically, fog clears as drier air is advected into the region from continental source regions to the west.

5.5 Air Quality

While there is occasional exposure to exhaust products from the existing offshore oil production facilities (Hibernia, Terra Nova, White Rose, and Hebron, all located in the Jeanne d'Arc Basin), helicopters, and supply vessels and other marine traffic, air quality in the Eastern NL offshore is anticipated to be good. The Eastern NL offshore area also receives long-range contaminants from the United States (originating from the Northeast Seaboard and industrial Midwest) (ExxonMobil Canada Properties 2011). No site-specific ambient air quality data exist for the Project Area.

The National Pollutant Release Inventory (NPRI) Reporting program data search was accessed to acquire data that characterizes the existing ambient air quality in offshore NL. The Canadian Environmental Protection Act (CEPA) regulates the NPRI Reporting program for criteria air contaminants (CACs) (carbon monoxide (CO), nitrogen dioxide (NO_2), sulphur dioxide (SO_2), particulate matter less than 2.5 and

10 microns in diameter ($PM_{2.5}$, PM_{10}), total particulate matter (TPM), and volatile organic compounds (VOCs)). Facilities must annually report their CAC emissions if they meet specified reporting triggers, The 2017 reporting year CAC emissions from the Hibernia, Terra Nova, White Rose, and Hebron platforms are provided in Table 5.8.

Table 5.8 2017 Facility Reported CAC Emissions (NPRI Reporting) – Newfoundland and Labrador Offshore Area Production Platforms

Facility	Air Emissions (tonnes/year)					
	CO	NO_2	TPM	PM_{10}	$PM_{2.5}$	VOC
Hibernia	1,740	1,113	175	174	174	1,005
Terra Nova	694	2,183	208	204	204	2,642
White Rose (Sea Rose FPSO)	505	2,782	130	130	130	422
Hebron	141	53	17	16	16	58

Source: ECCC 2019a
Note: SO_2 (and hydrogen sulphide) emissions have not been reported as the Jeanne d'Arc Basin is not known to contain sour gas.

Existing offshore oil production platforms are required to report their greenhouse gases (GHGs) annually to the GHG Emissions Reporting Program. The 2017 reporting year GHG from the Hibernia, Terra Nova, White Rose, and Hebron platforms are provided in Table 5.9.

Table 5.9 2017 Facility Reported GHG Emissions – Newfoundland and Labrador Offshore Area Production Platforms

Facility	GHG Emissions (tonnes CO_2 eq/year)			
	CO_2	CH_4	N_2O	Total
Terra Nova	587,587	32,444	9,774	629,806
Hibernia	536,172	41,475	3,298	580,945
White Rose	378,666	26,968	12,447	418,081
Hebron	22,732	4,547	404	27,684

Source: ECCC 2019b

The International Maritime Organization (IMO) (via MARPOL) regulates emissions from vessel traffic, which could also occasionally influence air quality in the vicinity of the Project Area.

5.6 Oceanography

5.6.1 Waves

The main parameters for describing wave conditions are the significant wave height, the maximum wave height, the peak spectral period, and the characteristic period. The significant wave height is defined as the average height of the ⅓ highest waves, and its value roughly approximates the characteristic height observed visually. The maximum height is the greatest vertical distance between a wave crest and adjacent trough. The spectral peak period is the period of the waves with the largest energy levels; the characteristic period is the period of the ⅓ highest waves.

A sea state may be composed of wind wave alone, swell alone, or wind wave in combination with one or more swell groups. A swell is a wave system not produced by the local wind blowing at the time of observation and may have been generated within the local weather system, or from within distant weather systems. The former situation typically arises when a front, trough, or ridge crosses the point of concern, resulting in a marked shift in wind direction. Swells generated in this manner are usually of low period. Swells generated by distant weather systems may propagate in the direction of the winds that originally produced the waves to the vicinity of the observation area. These swells may travel for thousands of miles before dying away. As the swell advances, its crest becomes rounded and its surface smooth. As a result of the latter process, swell energy may propagate through a point from more than one direction at a time.

The wave climate of the Grand Banks is dominated by extra-tropical storms, primarily during October through March. Severe storms may, on occasion, occur outside these months. Storms of tropical origin may occur during the early summer and early winter, but most often from late August through October. Hurricanes are usually reduced to tropical storm strength or evolve into extra-tropical storms by the time they reach the area, but they are still capable of producing storm force winds and high waves.

During autumn and winter, the dominant direction of the combined significant wave height is from the west. This corresponds with a higher frequency of occurrence of the wind wave during these months, suggesting that during the late fall and winter, the wind wave is the main contributor to the combined significant wave height. During the months of March and April, the wind wave remains predominantly westerly while the swell begins to come from a southerly direction, resulting in the vector mean direction of the combined significant wave heights being south-westerly. A mean south-westerly direction for the combined significant wave heights during the summer months is a result of a mainly south-westerly wind wave and a south-westerly swell. As winter approaches again, during the months of September and October, the wind wave will veer to the west and become the more dominant component of the combined significant wave height. This will result in the frequency of occurrence of the combined significant wave heights being westerly once again.

The MSC50 data set is used to analyze wave climate statistics for the Project Area. A 30-year subset of the MSC50 data from 1986 to 2015 is extracted for the analysis. Grid point 13741 (48.2°N and 47.3°W) is chosen to represent conditions within the area of interest.

An annual wave rose from the MSC50 grid point is presented in Figure 5-12. The wave rose is in oceanographic convention and depicts the direction the waves move towards. Therefore, the wave rose shows that most of the wave energy comes from southwest and northwest.

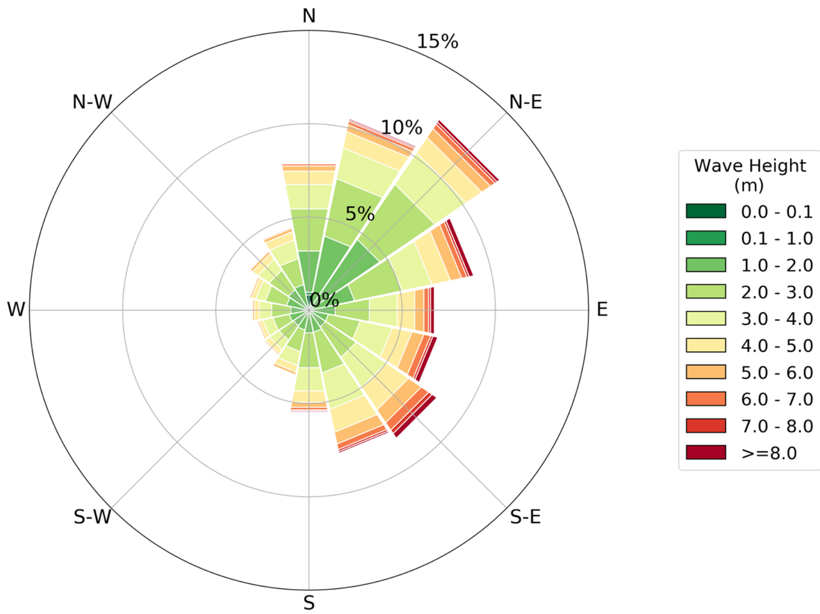

Figure 5-12 Annual Wave Rose for MSC50 Grid Point 13741 (1954 to 2015)

The annual percentage frequency of significant wave height is presented in Figure 5-13. The majority of significant wave heights lie between 1.0 and 3.0 m. There is a gradual decrease in frequency of wave heights above 3.0 m and only a small percentage of the wave heights exceed 7.0 m.

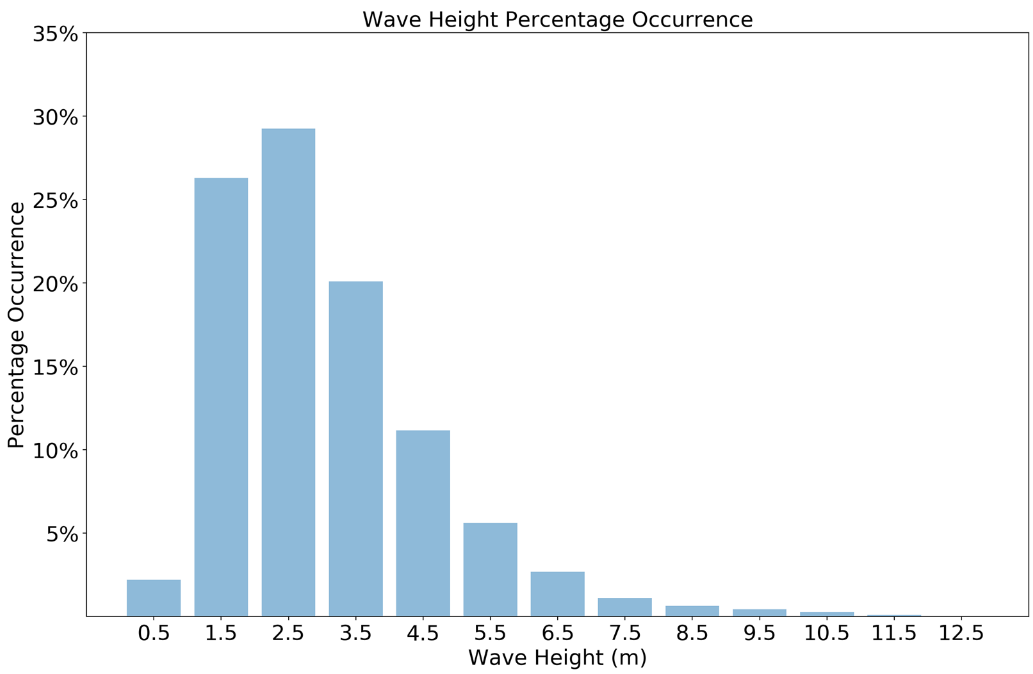

Figure 5-13 Annual Percentage Frequency of Wave Height for MSC50 Grid Point 13741 (1954 to 2015)

Significant wave height in the Project Area peaks during the winter months (Table 5.10). The mean monthly significant wave height reaches 4.6 m in January. The lowest significant wave height occurs in the summer, with July having a smallest mean monthly significant wave height of 1.8 m.

Table 5.10 Mean, Maximum and Standard Deviation of Significant Wave Height (m) Statistics for MSC50 Grid Point 13741 (1954 to 2015)

Month	Mean	Maximum	Standard Deviation
January	4.6	14.0	1.8
February	4.0	14.5	1.8
March	3.4	11.8	1.6
April	2.9	11.0	1.3
May	2.3	8.7	0.9
June	2.1	7.6	0.8
July	1.8	6.0	0.6
August	1.9	7.3	0.8
September	2.6	13.4	1.1
October	3.2	11.5	1.3
November	3.7	12.8	1.6
December	4.3	14.5	1.7

Maximum significant wave heights of 11.0 m or more occur in each month between September and April, with the highest waves of 14.5 m occurring during the months of February and December. The highest significant wave height of 14.54 m occurred during a storm event on February 12, 2003. The second highest significant wave height of 14.47 occurred on December 16, 1997. While the maximum significant wave heights tend to peak during the winter months, a tropical system could pass through the area and produce high wave heights during any month.

The percentage exceedance curve of significant wave heights is shown in Figure 5-14. The significant wave heights during winter months are larger than those during the rest of year.

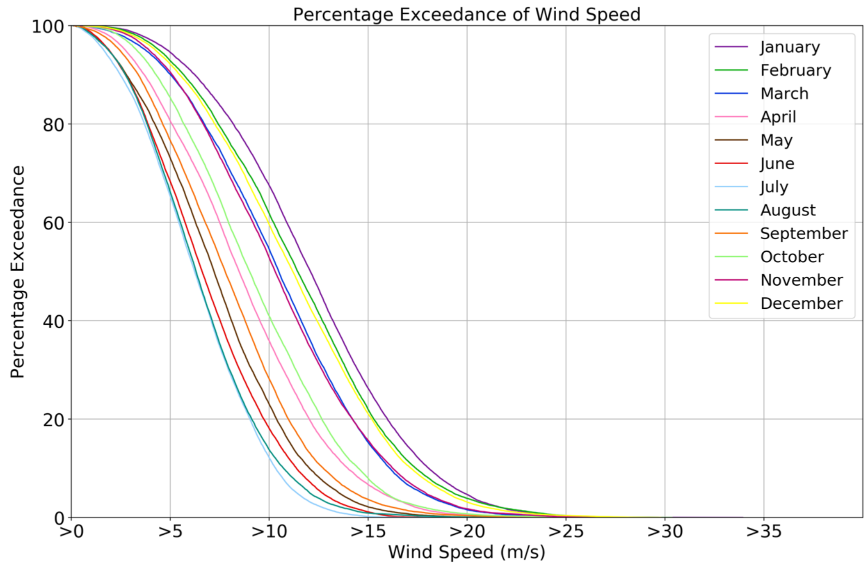

Figure 5-14 Percentage Exceedance of Significant Wave Height for MSC50 Grid Point 13741 (1954 to 2015)

The spectral period of waves varies with season with the most common period varying from 7-8 seconds during summer to 10-11 seconds in winter (Figure 5-15 and Table 5.11). Annually, the most common spectral peak period is 9 seconds. The percentage occurrence of spectral peak period for each month is shown in Table 5.12. The highest percentage for each month in the table is highlighted.

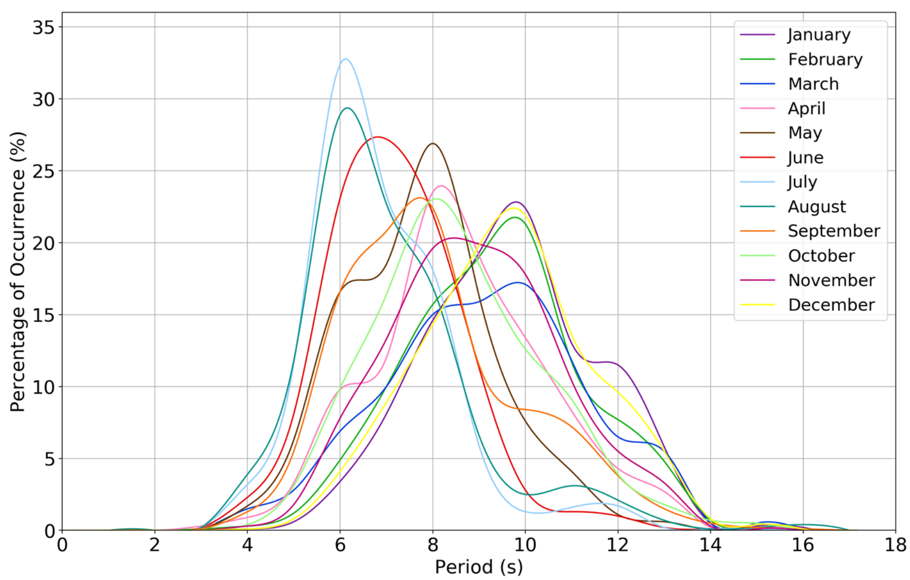

Figure 5-15 Percentage Occurrence of Peak Spectral Period of the Total Spectrum at MSC50 Grid Point 13741 (1954 to 2015)

Table 5.11 Percentage Occurrence of Peak Spectral Period of the Total Spectrum at MSC50 Grid Point 13741 (1954 to 2015)

Month	Peak Spectral Period (seconds)																	
	1	2	3	4	5	6	7	8	9	10	11	12	13	14	15	16	17	18
January	0.0	0.0	0.0	0.0	0.1	0.6	3.4	8.1	14.6	19.3	22.4	13.0	11.5	5.8	0.5	0.3	0.2	0.0
February	0.0	0.0	0.0	0.1	0.3	1.2	4.9	10.0	15.7	19.0	21.3	11.7	7.7	4.8	0.7	0.2	0.0	0.0
March	0.0	0.0	0.0	0.1	1.5	2.8	6.9	10.0	15.0	15.9	17.1	11.8	6.5	5.5	0.5	0.5	0.0	0.0
April	0.0	0.0	0.0	0.3	0.9	3.3	9.8	12.0	23.5	19.1	13.4	8.3	4.3	2.7	0.2	0.2	0.0	0.0
May	0.0	0.0	0.0	0.1	1.7	6.3	16.6	18.5	26.9	16.3	7.6	4.1	1.1	0.6	0.0	0.0	0.1	0.0
June	0.0	0.0	0.0	0.2	2.3	8.1	23.1	27.2	22.0	11.3	2.8	1.3	1.0	0.2	0.1	0.2	0.0	0.0
July	0.0	0.0	0.0	0.2	3.2	11.6	32.4	23.3	18.1	5.9	1.3	1.6	1.7	0.2	0.1	0.1	0.0	0.0
August	0.0	0.0	0.0	0.2	3.9	11.8	28.9	22.7	16.9	6.6	2.5	3.1	2.1	0.7	0.1	0.2	0.4	0.0
September	0.0	0.0	0.0	0.1	1.3	5.5	16.6	20.8	22.4	11.5	8.4	7.2	3.8	1.5	0.5	0.2	0.1	0.0
October	0.0	0.0	0.0	0.0	0.4	3.1	9.9	16.4	23.0	18.5	12.6	9.1	3.9	1.8	0.7	0.5	0.0	0.0
November	0.0	0.0	0.0	0.0	0.3	1.8	7.8	13.3	19.6	19.9	17.8	10.4	5.5	3.3	0.3	0.1	0.0	0.0
December	0.0	0.0	0.0	0.0	0.1	0.8	4.1	8.9	14.3	19.8	21.9	13.6	9.6	5.5	0.8	0.4	0.1	0.0
Annual	0.0	0.0	0.0	0.1	1.3	4.8	13.8	16.0	19.3	15.2	12.4	7.9	4.9	2.7	0.4	0.3	0.1	0.0

Table 5.12 Percentage Frequency of Occurrence of Significant Combined Wave Height and Peak Spectral Period at MSC50 Grid Point 13741 (1954 to 2015)

		Wave Height (m)															
		<1	**1**	**2**	**3**	**4**	**5**	**6**	**7**	**8**	**9**	**10**	**11**	**12**	**13**	**14**	**Total**
Period (s)	0	0.83															0.83
	1																0.00
	2																0.00
	3																0.00
	4		0.10	0.02													0.12
	5		0.62	0.68	0.03												1.33
	6		1.16	3.20	0.40	0.02											4.78
	7		3.65	6.12	3.64	0.35	0.02										13.78
	8		2.85	5.60	4.97	2.35	0.17	0.01									15.95
	9		1.67	**7.73**	4.35	4.20	1.29	0.08	0.01								19.33
	10		0.73	4.17	4.18	2.70	2.56	0.81	0.06								15.21
	11		0.21	1.83	4.01	2.56	1.64	1.52	0.54	0.08							12.39
	12		0.28	1.62	1.72	1.45	0.87	0.70	0.63	0.42	0.20	0.03					7.92
	13		0.20	0.62	0.88	0.92	0.69	0.46	0.26	0.24	0.27	0.24	0.08				4.86
	14		0.04	0.15	0.47	0.77	0.52	0.28	0.12	0.08	0.05	0.09	0.09	0.05	0.01		2.72
	15		0.01	0.04	0.04	0.04	0.10	0.07	0.03	0.01				0.02	0.01		0.37
	16		0.02	0.04	0.06	0.05	0.05	0.02	0.01						0.01	0.01	0.27
	17		0.02	0.03	0.01	0.01	0.01										0.08
	Total	0.83	11.56	31.85	24.76	15.42	7.92	3.95	1.66	0.83	0.52	0.36	0.17	0.07	0.03	0.01	99.4

Note: The incidence of 0 wave height and <1 wave period is due to the presence of sea ice.

5.6.2 Ocean Currents

The Labrador Current is the dominant current in the research area. The Labrador Current is composed of the West Greenland, Baffin Island Currents and Irminger Current. The currents on the Newfoundland Slope are highly variable due to the influences of strong atmospheric forcing, large inflows of sea ice, and interactions with the Gulf Stream and North Atlantic Current (Han and Li 2004). This results in the Labrador Current having seasonal and interannual variations in velocity and transport. Typically, the upper waters of the Labrador Current are stronger in fall and winter and weaker in spring (Lazier and Wright 1993; Han and Tang 1999; Han and Li 2004). Lazier and Wright (1993) found seasonal variations in the upper 400 m level circulation and no substantial variations deeper than the 1,000 m level.

The Labrador Current flows southward until it reached the southern part of Orphan Basin, where it is diverted eastward by the bathymetry. Upon reaching the entrance to Flemish Pass, the current divides into two branches. One branch continues to flow eastward north of Flemish Cap and the other branch flows southward through Flemish Pass.

Moored current measurements in West Flemish Pass have been carried out by the Bedford Institute of Oceanography (BIO) in the past decades. Current moorings selected for this report in are described in the following section.

Six moored current measurements were made in West Flemish Pass between April 11, 1976 and May 07, 2010. All mooring sites are close to EL 1138. The locations of these moorings are listed in Table 5.13 and shown in Figure 5-16.

Progressive vector diagrams for moorings 1 to 6 at different depth levels are presented in Appendix 5A; Figures 1-1 to 1-6. For Mooring 1, currents flowed towards a southerly direction at all three depth (467 m, 767 m, and 927 m). For Mooring 2 and Mooring 4, currents flowed towards east at all depths. Currents at locations of Mooring 3, Mooring 5, and Mooring 6 flowed in east-southeast directions.

Table 5.13 BIO Current Meter Data for the Project Area - West Flemish Pass (1976 to 2010

Mooring #	Date	Instrument Depth (m)	Latitude	Longitude
1	Apr 11, 1976 – Jul 17, 1976	467	47.9943N	47.1101W
		767		
		927		
2	Jun 03, 2004 – May 23, 2005	702	48.3290N	47.8085W
	Jan 29, 2005 – May 23, 2005	1502		
	Jun 03, 2004 – May 23, 2005	1902		
3	Jun 04, 2004 – May 22, 2005	361	48.5388N	47.6903W
		711		
		1111		
		1511		
		1911		
		2236		
4	May 23, 2005 – May 17, 2006	1907	48.3295N	47.8088W
5	May 11, 2008 – May 08, 2009	363	48.5496N	47.6507W

Table 5.13 BIO Current Meter Data for the Project Area - West Flemish Pass (1976 to 2010

Mooring #	Date	Instrument Depth (m)	Latitude	Longitude
	May 12, 2008 – Apr 26, 2009	713		
	May 12, 2008 – May 08, 2009	1113		
	May 11, 2008 – May 08, 2009	1513		
	May 12, 2008 – Oct 24, 2008	1913		
	May 12, 2008 – Dec 29, 2008	2263		
6	May 09, 2009 – May 07, 2010	337	48.5493N	47.6479W
	May 09, 2009 – May 07, 2010	687		
	May 08, 2009 – May 07, 2010	1087		
	May 08, 2009 – Jan 31, 2010	1487		
	May 09, 2009 – May 07, 2010	1887		
	May 09, 2009 – May 07, 2010	2212		

The summary of statistics of current data collected at Moorings 1 to 6 from April 11, 1976 to May 07, 2010 are presented in Table 5.14. The statistics of current at West Flemish Pass moorings 1 to 6 are provided in Appendix E; Tables 1.1 to 1.6.

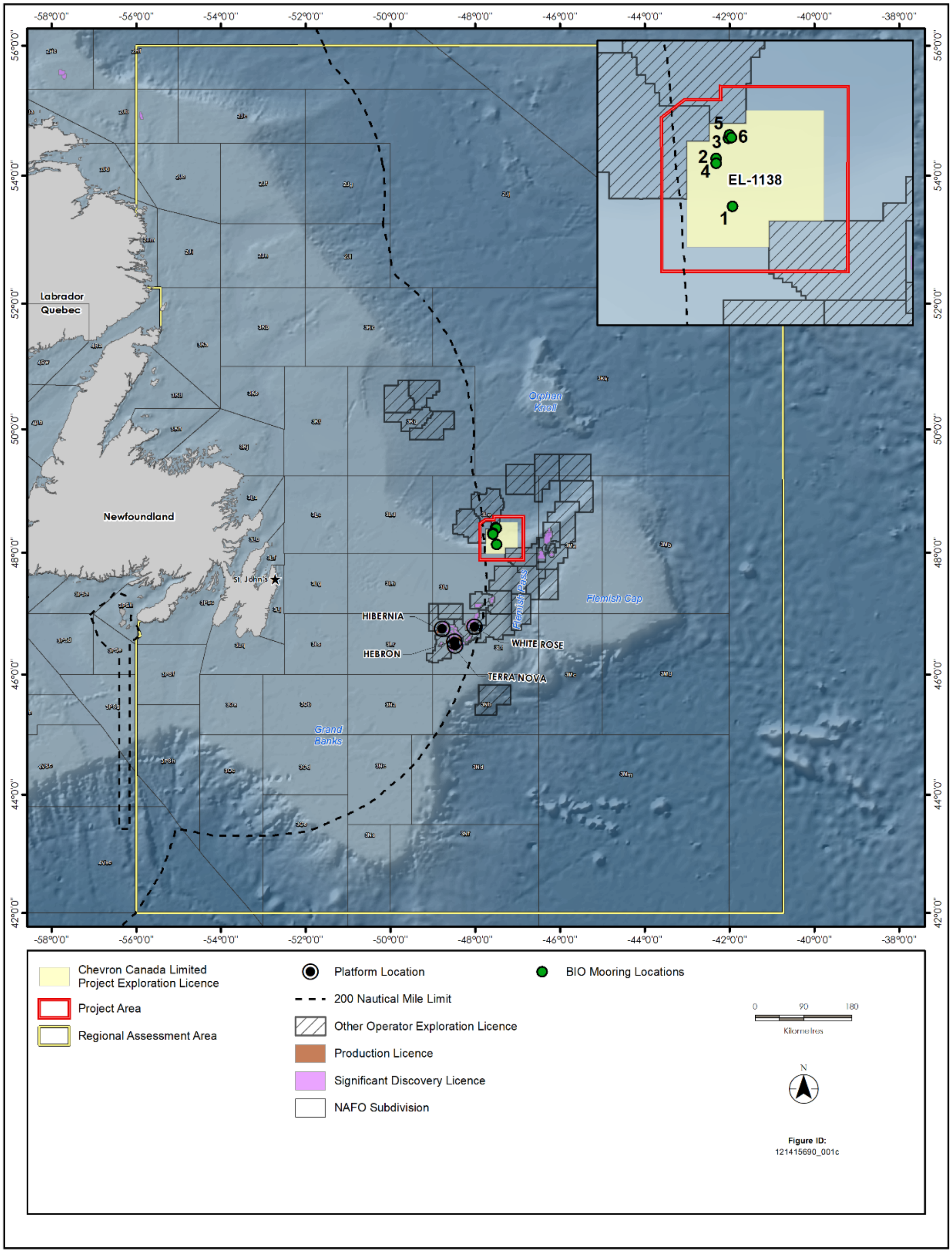

Figure 5-16 BIO Mooring Locations at West Flemish Pass (1976 to 2010)

Table 5.14 Summary of Statistics of Current at West Flemish Pass (1976 to 2010)

Mooring #	Depth (m)	Max Speed (cm/s)	Mean Speed (cm/s)	Mean Velocity (cm/s)	Direction of Mean Velocity (T)
1	467	27.2	8.1	5.9	181
	767	37.3	8.3	6.7	188
	927	3	1.5	1.3	169
2	702	45	14.4	13.4	98
	1502	30.7	11.2	10.1	95
	1902	27.3	7.7	5.6	89
3	361	47.9	12.1	10.3	108
	711	46.3	9.6	8.5	113
	1111	36.8	11.0	9.8	116
	1511	28.4	9.4	8.4	111
	1911	31.3	9.0	7.9	111
	2236	29.3	9.5	7.9	101
4	1907	24.1	6.6	4.5	86
5	363	54.9	13.2	10.9	111
	713	48.1	11.5	9.6	106
	1113	36.6	11.7	10.1	111
	1513	29.3	8.5	7.5	112
	1913	24.3	6.4	5.3	109
	2263	39.9	9.0	7.8	117
6	337	30.7	13.3	12.4	108
	687	24.2	9.4	8.9	109
	1087	27.5	12.1	11.4	111
	1487	24.2	9.9	9.2	109
	1887	23.5	10.2	9.3	105
	2212	27.6	10.6	9.1	114

5.6.3 Extreme Events

Extreme wind and waves are calculated for the Project Area using the MSC50 hindcast data set. This data set is determined to be the most representative of the available data sets, as it provides a continuous wind and wave hindcast in 1-hour time steps from January 1954 to December 2015, on a 0.1° latitude by 0.1° longitude grid. All extremes are specified for return periods of 1-year, 10-year, 25-year, 50-year and 100-year. All wind speeds are referenced to the 10 m height.

The extreme value analysis for wind speeds is carried out using the peak-over-threshold method. For the extreme wave analysis, two methods are used: the peak-over-threshold method and the joint probability method.

After considering four different distributions, the Gumbel distribution is chosen to be the most representative for the peak-over-threshold method as it provides the best fit to the data. Since extreme values can vary depending how well the data fits the distribution, a sensitivity analysis using Oceanweather's Osmosis software program is carried out to determine the number of storms to use, whereby the number of storms, the 100-year extreme value, the correlation coefficient and storm threshold are all compared on an annual and monthly basis. The number of storms determined to be used in the following extreme analysis is presented in Table 5.15.

Table 5.15 Number of Storms Providing Best Fit for Extreme Value Analysis of Winds and Waves

Component	Annual	Monthly
Wind	265	93
Wave	238	86

The methodological description of the Gumbel extreme value analysis of wind and waves is provided in Appendix E; Section 2.

5.6.3.1 Extreme Winds

The extreme value estimates for wind are calculated using Oceanweather's Osmosis software program for the return periods of 1-year, 10-year, 25-year and 100-year. The analysis used hourly wind values for the reference height of 10 m above sea level. The calculated extreme values are then converted to values corresponding to 10-minute and 1-minute wind speeds using a constant ration of 1.06 and 1.22, respectively (US Geological Survey 1979).

The calculated annual and monthly values for 1-hour, 10-minute and 1-minute are presented in Table 5.16. The annual 100-year extreme 1-hour wind speed is 32.81 m/s. The highest extreme monthly wind occurs during February with a 100-year extreme wind estimate of 31.75 m/s.

Table 5.16 Extreme Wind Speed Estimates (m/s) for Return Periods of 1, 10, 25, 50 and 100 Years

Month	Wind Speed 1-hr (m/s)					Wind Speed 10-min (m/s)					Wind Speed 1-min (m/s)				
	1	10	25	50	100	1	10	25	50	100	1	10	25	50	100
JAN	22.94	27.44	28.96	30.10	31.23	24.32	29.09	30.70	31.91	33.10	27.99	33.48	35.33	36.72	38.10
FEB	22.75	27.63	29.28	30.52	31.75	24.12	29.29	31.04	32.35	33.66	27.76	33.71	35.72	37.23	38.74
MAR	20.84	25.28	26.79	27.91	29.03	22.09	26.80	28.40	29.58	30.77	25.42	30.84	32.68	34.05	35.42
APR	18.59	23.11	24.64	25.78	26.92	19.71	24.50	26.12	27.33	28.54	22.68	28.19	30.06	31.45	32.84
MAY	16.14	20.55	22.04	23.16	24.26	17.11	21.78	23.36	24.55	25.72	19.69	25.07	26.89	28.26	29.60
JUN	14.95	18.36	19.52	20.38	21.24	15.85	19.46	20.69	21.60	22.51	18.24	22.40	23.81	24.86	25.91
JUL	13.57	16.37	17.32	18.03	18.73	14.38	17.35	18.36	19.11	19.85	16.56	19.97	21.13	22.00	22.85
AUG	14.41	20.19	22.15	23.61	25.06	15.27	21.40	23.48	25.03	26.56	17.58	24.63	27.02	28.80	30.57
SEP	17.48	23.30	25.27	26.74	28.21	18.53	24.70	26.79	28.34	29.90	21.33	28.43	30.83	32.62	34.42
OCT	18.83	24.68	26.66	28.14	29.61	19.96	26.16	28.26	29.83	31.39	22.97	30.11	32.53	34.33	36.12
NOV	20.35	24.80	26.31	27.43	28.55	21.57	26.29	27.89	29.08	30.26	24.83	30.26	32.10	33.46	34.83
DEC	22.08	26.88	28.50	29.71	30.92	23.40	28.49	30.21	31.49	32.78	26.94	32.79	34.77	36.25	37.72
ALL	25.83	29.40	30.76	31.78	32.81	27.38	31.16	32.61	33.69	34.78	31.51	35.87	37.53	38.77	40.03

5.6.3.2 Extreme Waves

The annual and monthly extreme value estimates for significant wave height for return periods of 1-year, 10-year, 25-year, 50-year and 100-year are given in Table 5.17. The annual 100-year extreme significant wave height is 15.5 m. Monthly, the highest extreme significant wave height occurs during the month of February with an extreme height of 15.3 m.

Table 5.17 Extreme Significant Wave Height (m), Extreme Maximum Wave Height (m), and Associated Peak Period (s) Estimates for Return Periods of 1, 10, 25, 50 and 100 Years

Month	Significant Wave Height (m)					Maximum Wave Height (m)					Associated Peak Period (s)				
	1	10	25	50	100	1	10	25	50	100	1	10	25	50	100
JAN	9.7	12.5	13.4	14.1	14.7	19.9	23.6	24.8	25.8	26.7	12.9	14.7	15.2	15.6	16.0
FEB	9.1	12.5	13.7	14.5	15.3	19.1	24.0	25.7	26.9	28.1	12.7	14.7	15.4	15.8	16.2
MAR	7.4	10.1	11.1	11.7	12.4	15.2	19.6	21.1	22.2	23.3	11.7	13.3	13.8	14.1	14.4
APR	6.2	9.0	9.9	10.6	11.3	13.0	17.4	18.8	19.9	21.0	11.2	12.8	13.2	13.5	13.9
MAY	4.8	7.8	8.8	9.5	10.2	10.4	15.7	17.5	18.8	20.2	9.9	12.2	12.8	13.3	13.7
JUN	4.1	6.3	7.1	7.7	8.2	8,4	13.0	14.5	15.6	16.7	9.1	11.1	11.7	12.1	12.4
JUL	3.6	5.2	5.8	6.2	6.6	7.2	10.0	10.9	11.6	12.3	8.5	10.5	11.1	11.5	11.9
AUG	4.0	6.3	7.1	7.6	8.2	8.5	12.4	13.7	14.6	15.6	9.5	11.1	11.6	11.9	12.2
SEP	5.6	9.8	11.2	12.3	13.3	11.7	18.6	20.9	22.5	24.2	10.8	13.6	14.4	15.0	15.5
OCT	6.7	10.6	11.9	12.8	13.8	14.5	21.4	23.7	25.4	27.1	12.0	13.5	13.9	14.2	14.4
NOV	7.9	11.3	12.4	13.3	14.1	16.4	21.8	23.6	24.9	26.3	12.1	13.9	14.4	14.8	15.2
DEC	9.4	12.4	13.4	14.1	14.9	19.4	24.1	25.6	26.8	27.9	13.1	14.6	15.0	15.3	15.6
ALL	11.4	13.5	14.3	14.9	15.5	22.1	25.3	26.5	27.5	28.4	14.1	15.1	15.4	15.6	15.9

The maximum individual wave height and extreme associated peak periods are also presented in Table 5.18. Maximum individual wave height and the extreme associated peak periods are highest during the month of February.

Table 5.18 Annual Extreme Significant Wave Estimates and Spectral Peak Periods for Return Periods of 1, 10, 25, 50 and 100 Years using Hourly and 6-hourly Datasets

Return Period (years)	Hourly Dataset		6-Hourly Dataset	
	Significant Wave Height (m)	Spectral Peak Period Median Value (s)	Significant Wave Height (m)	Spectral Peak Period Median Value (s)
1	13.3	15.0	11.5	14.2
10	15.7	16.1	13.9	15.4
25	16.6	16.5	14.9	15.9
50	17.3	16.8	15.6	16.2
100	18.0	17.0	16.2	16.5

5.6.4 Seawater Properties (temperature, salinity, pH, turbidity)

Temperatures and salinity data from historical measurements were extracted from the BIO archive. Locations of these measurements are shown on Figure 5-17. These data are presented as monthly statistics. In West Flemish Pass, the water depth varies between 400 m and 2,300 m.

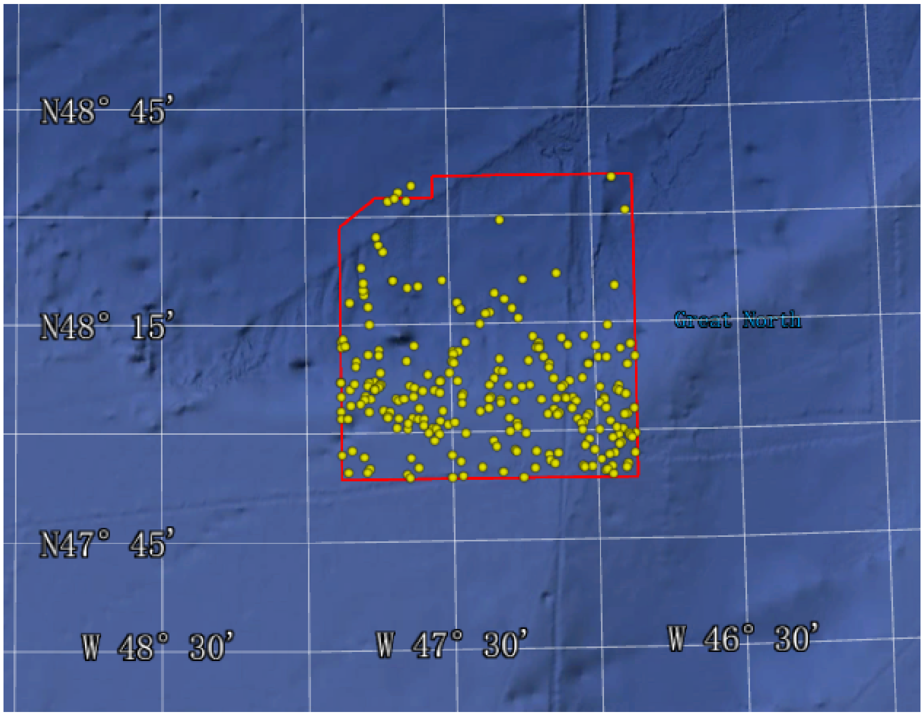

Figure 5-17 BIO Conductivity, Temperature and Depth Mooring Locations in the West Flemish Pass (1927 to 2009)

Summarized statistics of sea water temperature and salinity at depths of 0 m, 50 m, 100 m, 200 m, 300 to 900 m, and 1,000 to 3,000 m at West Flemish Pass are provided in Appendix E; Tables 2.1 to 2.6. The surface waters were warmest during the months of July to October with mean temperatures ranging from 6.88°C to 10.80°C. The coldest temperatures were in March and April with mean temperatures of -0.78°C and -0.15°C, respectively. The mean salinities ranged between 32.58 practical salinity unit (psu) in July and 34.07 psu in January. At a depth of 50 m, the mean temperatures ranged between -1.11°C in March to 5.10°C in October. The mean salinities ranged between 33.49 psu in March and 34.21 psu in July. At a depth of 100 m, the mean temperatures ranged between 0.71°C in March and 3.76°C in July and October. The mean salinity values ranged from 34.06 psu in June to 34.62 psu in July. At a depth of 200 m, the mean temperatures ranged between 2.31°C in March to 4.38°C in July. The mean salinity had no substantial difference among months with values that ranged from 34.55 psu in March and April and 34.82 psu in July and October. At a depth of 300 to 900 m, the mean temperatures ranged between 3.21°C in April to 3.93°C in November. The mean salinity values ranged from 34.77 psu to 34.87 psu. At a depth of 1,000 to 3,000 m, the mean temperatures ranged between 3.20°C in March to 3.57°C in May. The mean salinity values that ranged from 34.84 psu in December and 34.92 psu in April.

Figures 5-18 and 5-19 show the mean temperature and mean salinity by month. In summer, the surface water temperature is substantially higher than seawater at a deeper depth, while in January, February and March, surface seawater temperature is substantially lower than seawater temperature at near-bottom.

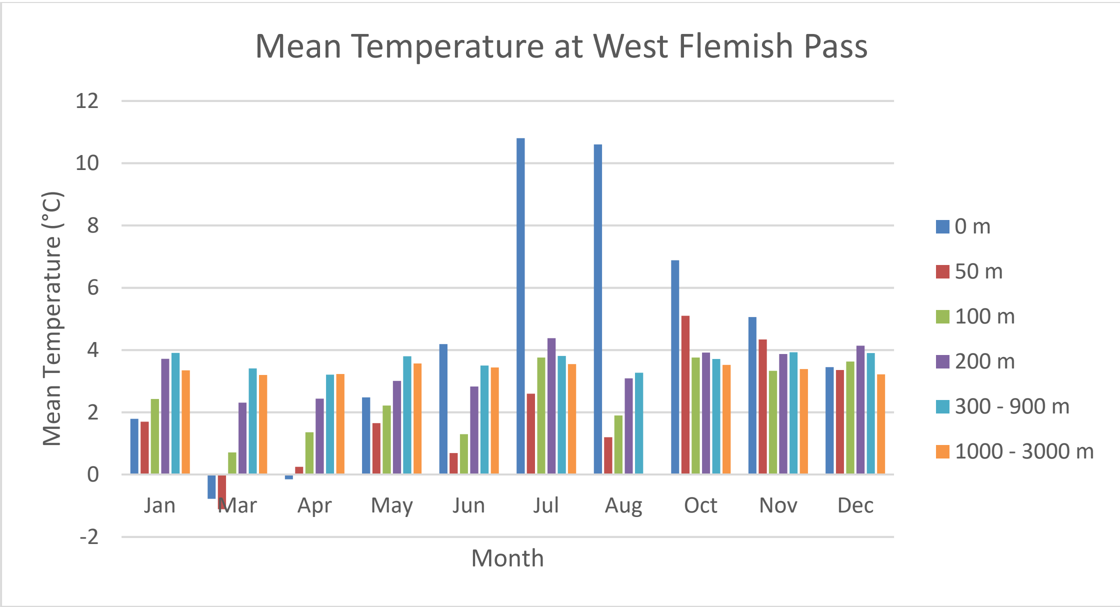

Figure 5-18 Mean Temperature at West Flemish Pass from Historical Conductivity, Temperature and Depth Data (1927 to 2009)

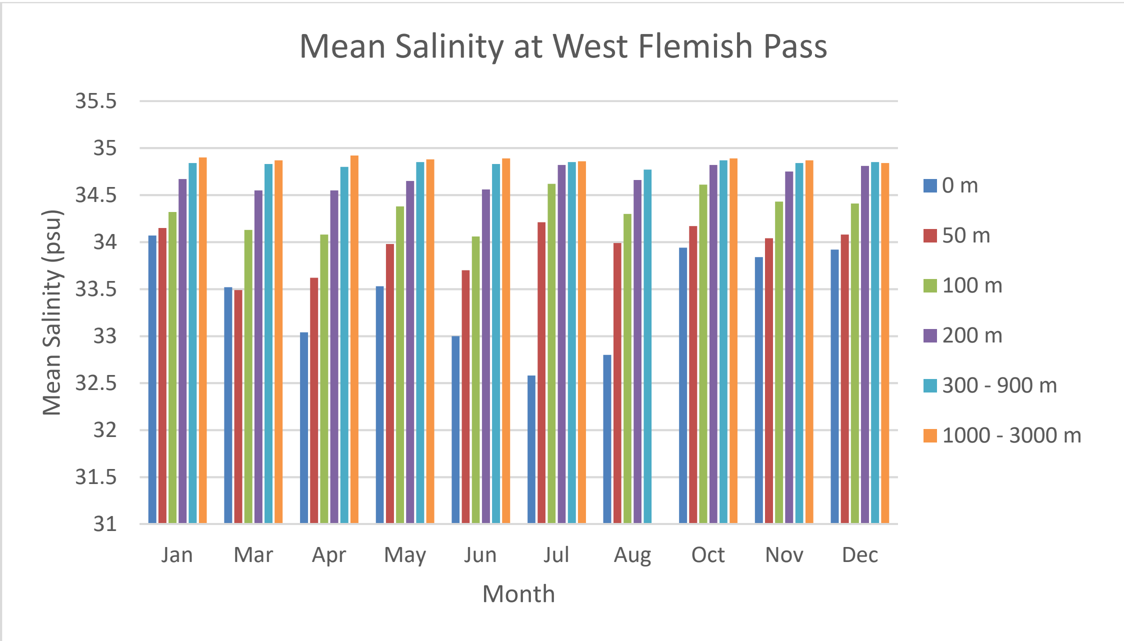

Figure 5-19 Mean Salinity at West Flemish Pass from Historical Conductivity, Temperature and Depth Data (1927 to 2009)

5.6.5 Tides

There are no tidal measurements for Flemish Pass. Tidal information for the Grand Banks comes from a tidal study carried out by the BIO in 1983-1984. From the BIO data, Petrie et al. (1987) prepared co-range and co-phase tidal charts for the Grand Banks for constituents M2, S2 and K1. By extrapolating the co-range lines, the M2 constituent for Flemish Pass is 25 cm and S2 and K1 has values of approximately 10 cm each. This means that the tidal height in Flemish Pass is expected to be approximately 50 cm.

5.6.6 Storm Surge

The water level due to storm surge is the inverse barometer effect due to the variation in atmospheric pressure plus the rise in sea level as a result of wind stress on the surface of the ocean. Severe storm surges can cause the ocean to rise by a few meters in coastal regions, but much smaller in the absence of a boundary. The extreme 100-year return period storm surge value near Terra Nova was calculated by Seaconsult (1988) as being 73 cm above mean water level.

The inverse barometer effect causes a sea level rise of 1 cm/1 mb as the atmospheric pressure drops. The minimum atmospheric pressure measured in Flemish Pass over the last 15 years was 952.0 mb on February 20, 2007, and again during Hurricane Igor on September 22, 2010. This gives a sea level rise of approximately 56 cm. The total storm surge level will be somewhat higher due to the effect of wind stress.

Bernier and Thompson (2006) did a modelling study of storm surges and extreme sea levels in the Northwest Atlantic. Figure 5-20 shows that the 40-year return level of extreme storm surges in West Flemish Pass is 70 to 80 cm for this return period.

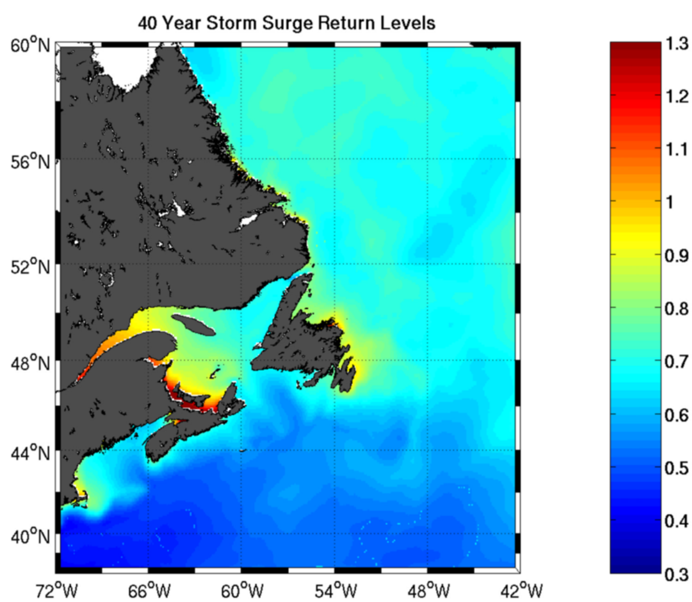

Source: Bernier and Thompson 2006
Note: Colour bar indicates the 40-year return levels in metres

Figure 5-20 40-year Return Level of Extreme Storm Surges based on the Surge Hindcast

5.7 Lightning

Lightning strikes in offshore Newfoundland occur year-round but are typically stronger in winter. Lightning is usually accompanied by thunder as it is most commonly produced in thunderstorms (Statoil Canada Ltd. 2017).

There is no information on lightning activity in the Project Area given offshore location. The Canadian Lightning Detection Network provides Land-based measurements and statistics for the Newfoundland and Labrador region are available from a study by the Canadian Lightning Detection Network (conducted between 1999 to 2013 (Table 5.19).

Table 5.19 Lightning Activity in Newfoundland and Labrador (1999 to 2013)

City	Area (km^2)	Total Lightning Strikes from 1999 to 2013	Average Number of Days with Lightning (within 25 km)
Labrador City	38.83	2,231	8.1
Grand Falls-Windsor	54.48	2,747	7.6
Corner Brook	148.30	2,334	7.5
Goose Bay	305.80	1,133	6.8
Gander	104.20	2,579	6.7
Conception Bay South	59.27	644	4.6
Mount Pearl	15.76	580	4.2
Paradise	29.24	590	4.2
St. John's	446.06	566	4.1

Source: ECCC 2016 - Canadian Lightning Detection Network
Total lightning flashes are calculated within a 25 km radius of the centre of each locality

5.8 Underwater Sound

Sound from a point source emanates in a spherical pattern until it reaches the sea surface or seabed, at which point the spreading becomes cylindrical. Seabed conditions and bathymetry of the Project Area are discussed in Sections 5.1 and 5.3, respectively. Underwater sound modelling conducted for this Project (Zykov and Alavizadeh 2019) is provided in Appendix D.

A variety of natural and anthropogenic sources combine to create the ambient soundscape in the ocean (refer to Figure 5-21). The primary physical environment sources of sound are sea ice (main contributor), precipitation (a common contributor; typically concentrated at frequencies above 500 Hz), as is wind. Earthquakes and other geological events can also contribute low frequencies (<100 Hz) to the ambient soundscape. Anthropogenic sources of sound include vessel traffic (including military vessels), fishing activities (other than fishing vessel movement), and activities associated with oil and gas exploration and extraction (including air traffic / helicopters) (Delarue et al. 2018).

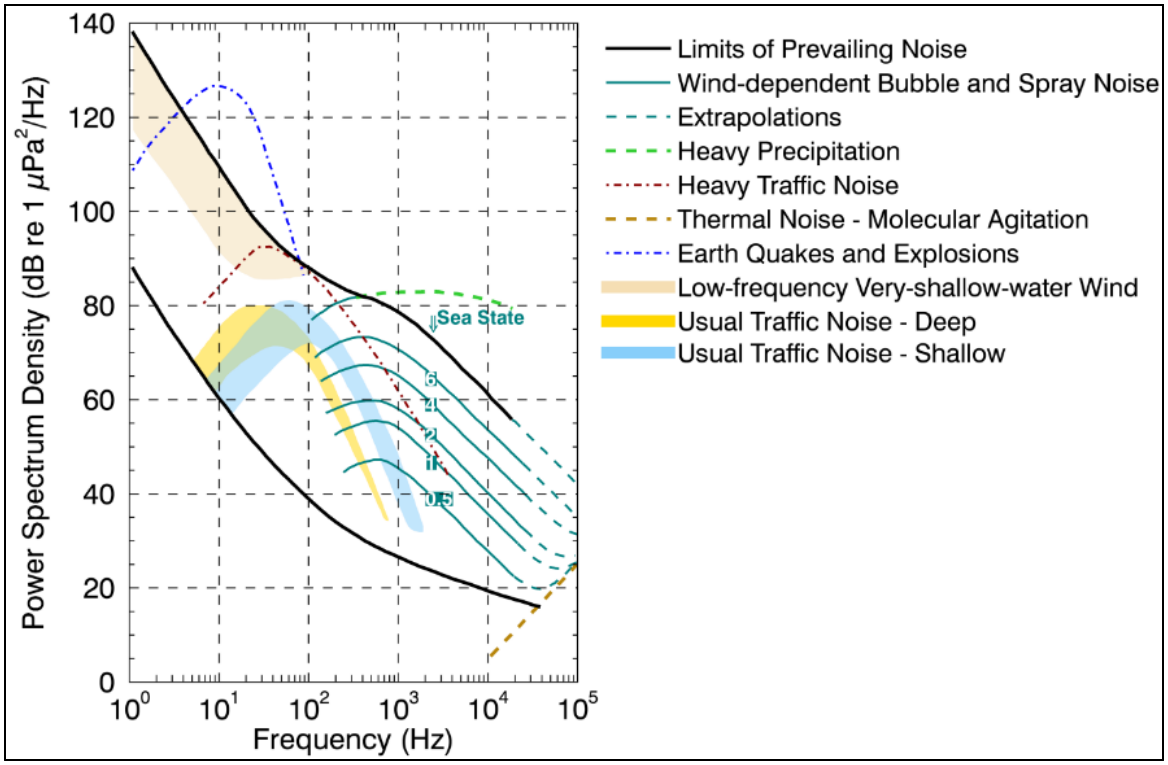

Source: adapted from Wenz (1962), in Delarue et al. 2018

Figure 5-21 Wenz Curves Describing Pressure Spectral Density Levels of Marine Ambient Noise from Weather, Wind, Geologic Activity, and Commercial Shipping

The Environmental Studies Research Fund (ESRF) conducted a two-year (2015-2017) recording program in shallow and deep water to characterize the east coast of Canada's underwater soundscape and the occurrence of marine mammals (Delarue et al. 2018). The study involved the deployment of 20 acoustic recorders from Nain Bank on the Labrador shelf to Dawson Canyon off Halifax, NS (Figure 5-22). Station 19 (orange dot in Figure 5-22, moved in 2016 due to repeated summer sightings of northern bottlenose whale in the Sackville Spur area) is closest to the Project Area.

Station 19 was deployed in the southeastern part of Orphan Basin (at a depth of 1547 m). The maximum and minimum broadband sound pressure levels (SPLs) measured at Station 19 in 2016-2017 were 157.6 and 95.5 dB re 1 μPa, respectively. The two main soundscape features were fin whale calls and seismic survey activity from July to October (Delarue et al. 2018).

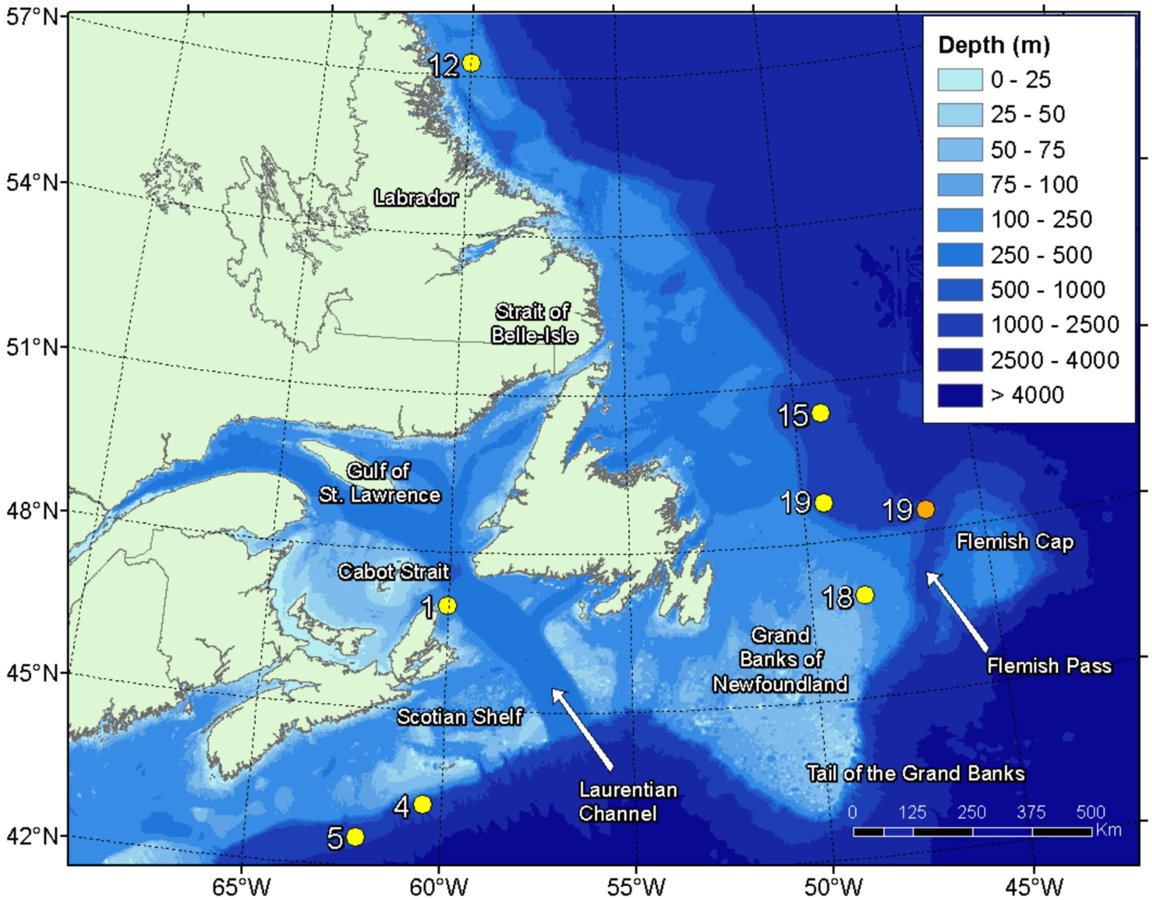

Source: Delarue et al. 2018

Note: The orange dot represents the location of Station 19 in 2016-2017

Figure 5-22 Key ESRF Study Station Locations for Ambient Marine Noise

Fin whale notes were detected from September to mid-March (although these were masked until seismic surveys ended in late October) and were the main source of identifiable sound. On the Grand Banks, fin whales sing from October to March and in winter and the total sound level across the Grand Banks can increase by 5 to 10 dB (in the 10 to 45 Hz band) by their constant notes. Vessel traffic is typically a transient sound source that is detectable over a period of several hours. Sounds from vessels (including DP MODUs) are continuously present closer to oil and gas activities (both exploration-related and production facilities), (Matthews et al. 2018).

Although the seismic surveys detected at Stations 15 and 19 were over 100 km from the recorders, they were still a dominant sound source in the soundscape. The peak frequency of sound from seismic source arrays is near 50 Hz (Dragoset 1984); however, the frequency range increases as the source vessel gets closer to a measurement location. The measurements reported in the ESRF Study included energy up to 1 kHz. This sound source is variable in space and time depending on where the seismic source is located. It is expected that 2D and 3D seismic surveys will continue off Newfoundland for the foreseeable future each summer.

5.9 Ice Conditions

5.9.1 Sea Ice

A weekly analysis of the Canadian ice Service's 30-year median of ice in North Atlantic reveals that ice is only present in Flemish Pass from mid-January until late May. Figures 5-23 to 5-25 shows the weekly analysis of 30-year median of ice concentration when ice is presented in Flemish Pass. The likelihood of ice present in Flemish Pass is highest during the week beginning February 5. During this week, the median of ice concentration in some are of Flemish Pass is 9-9+/10. Figure 5-26 indicates that the frequency of sea ice presence in the study areas is 1% to 15%. The potential exists for landfast ice in the nearshore. Landfast ice has the potential to influence conditions within the vessel transit route near to St. John's and Witless Bay; however, it is unlikely to be a factor in the Project Area itself.

5.9.2 Icebergs

Icebergs typically appear off the coast of Newfoundland by February or March and most icebergs are present from April to June or July. By the end of summer, most icebergs along the coast of Newfoundland have drifted south of the Grand Banks or have melted (AMEC 2011). The risk of iceberg collisions varies year to year. There have been years when no icebergs have been recorded passing across 48°N, while other years more than 1,000 icebergs are recorded (Bigg 2016). In 2017, there were over 1,000 icebergs counted in the shipping lanes off Newfoundland between February and July. In 2014 and 2015, there were 1,546 and 1,165 icebergs counted, respectively (CBC News 2017).

Figure 5-27 shows the distribution of the IIP iceberg sightings based on data collected from 1960 to 2017. The density of iceberg sightings shows that the east/west distribution of icebergs changes considerably with latitude. Icebergs along the Labrador coast (north of 55 ºN) tend to be concentrated along a relatively narrow band close to shore, 3 to 4 degrees of longitude wide. From northern Grand Banks, distribution of icebergs widens to a band that covers approximately 10 degrees of longitude. Iceberg count by years in the research area is presented in Figure 5-28. In 2015 and 2016 there are more icebergs in West Flemish Pass. Iceberg count by month in the research area is indicated in Figure 5-29. More icebergs were sighted in March, April and May than in the other months of the year.

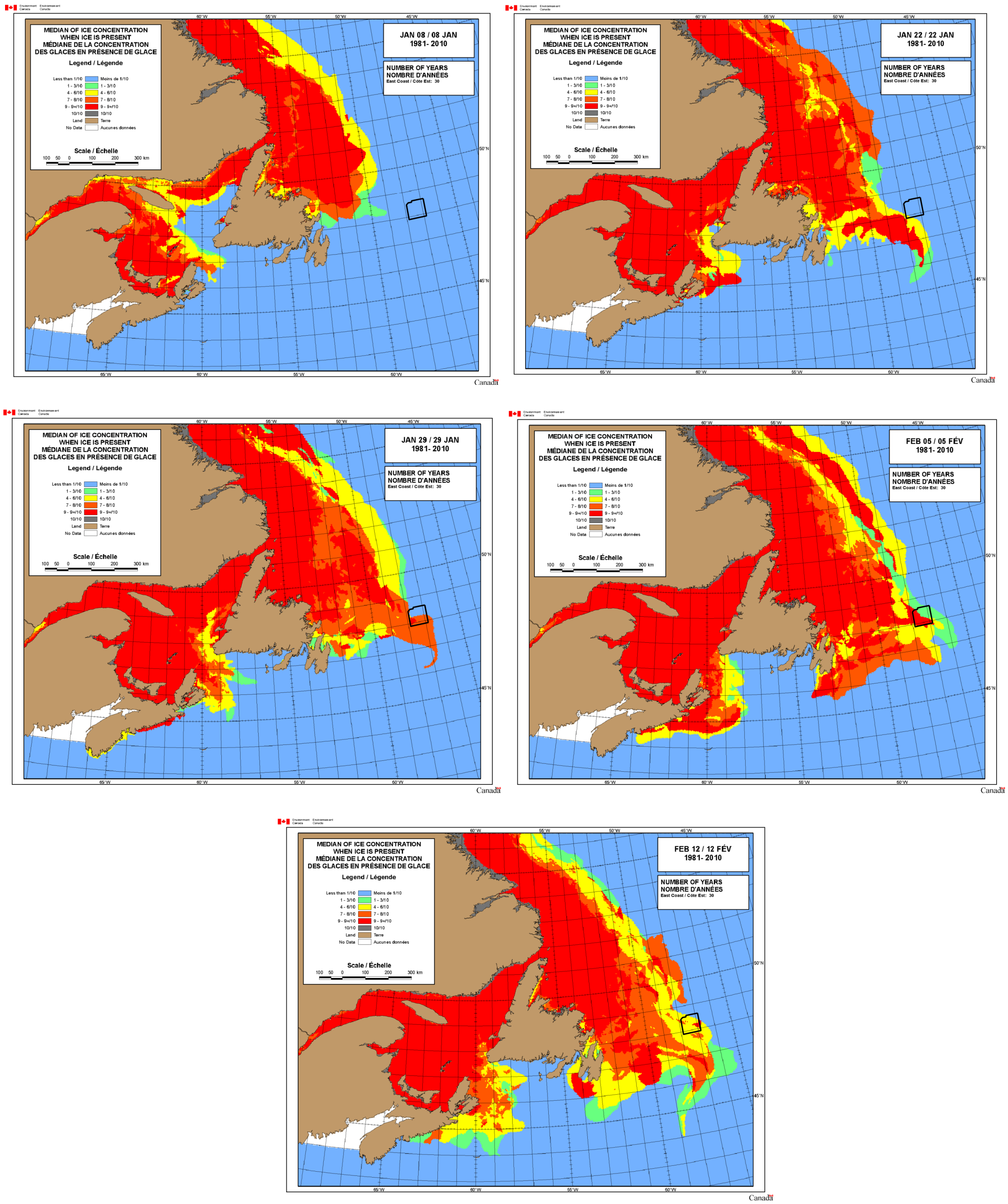

Source: Canadian Ice Service

Figure 5-23 Weekly Analysis of 30-year Median of Ice Concentration when Ice is Present in Flemish Pass (black polygon) from 1981-2010 (January to February)

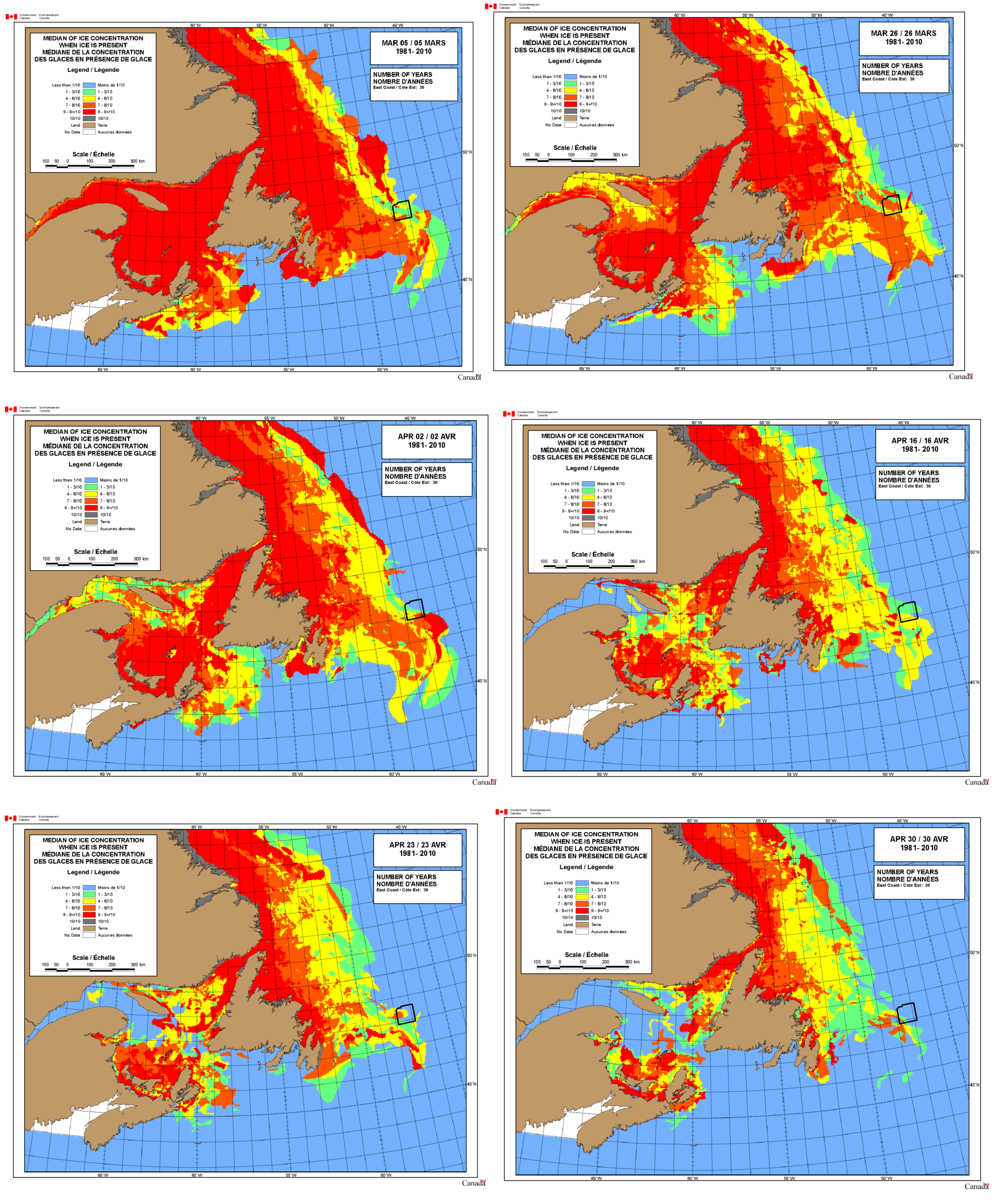

Source: Canadian Ice Service

Figure 5-24 Weekly Analysis of 30-year Median of Ice Concentration when Ice is Present in Flemish Pass (black polygon) from 1981-2010 (March to April)

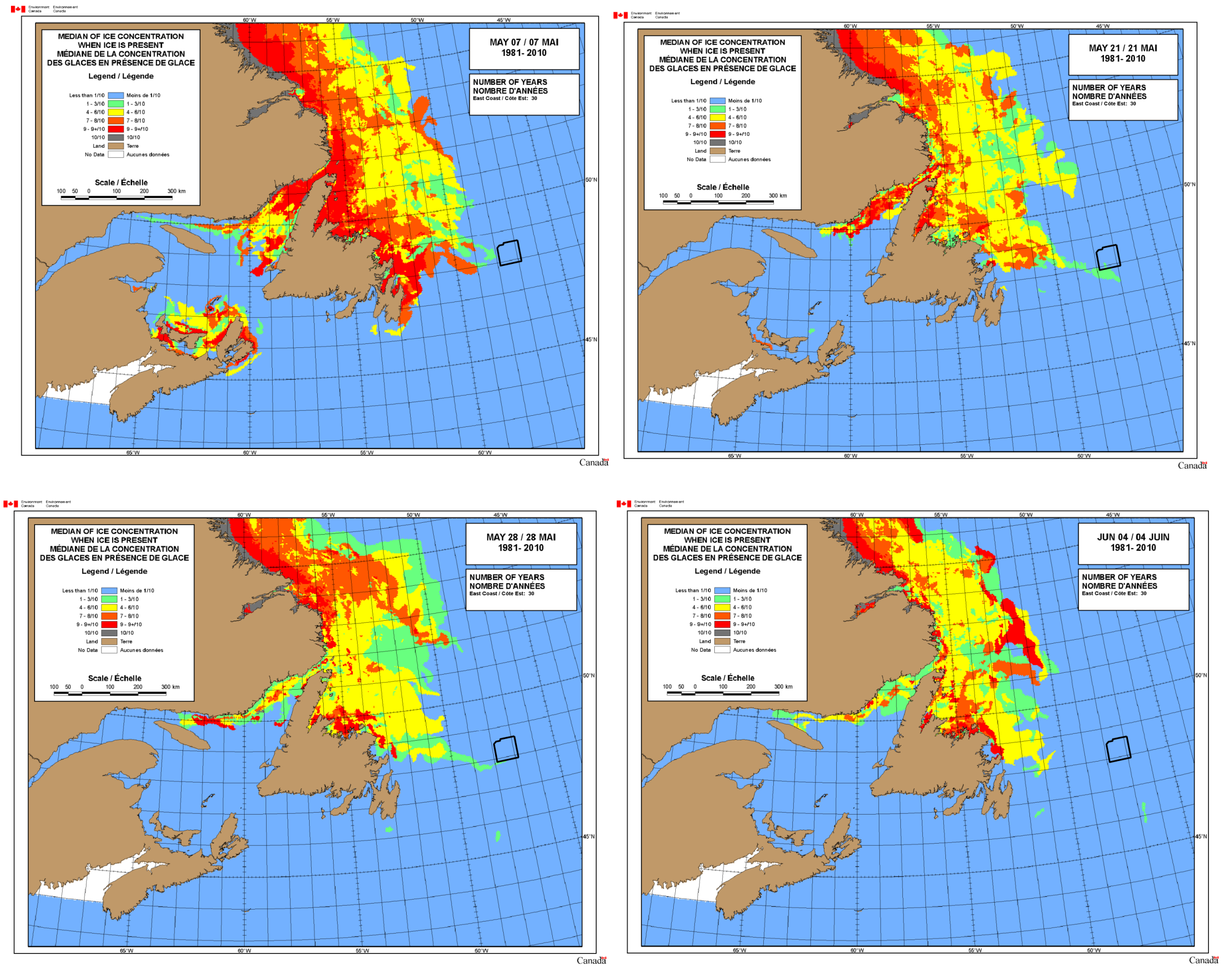

Source: Canadian Ice Service

Figure 5-25 Weekly Analysis of 30-year Median of Ice Concentration when Ice is Present in Flemish Pass (black polygon) from 1981-2010 (May to June)

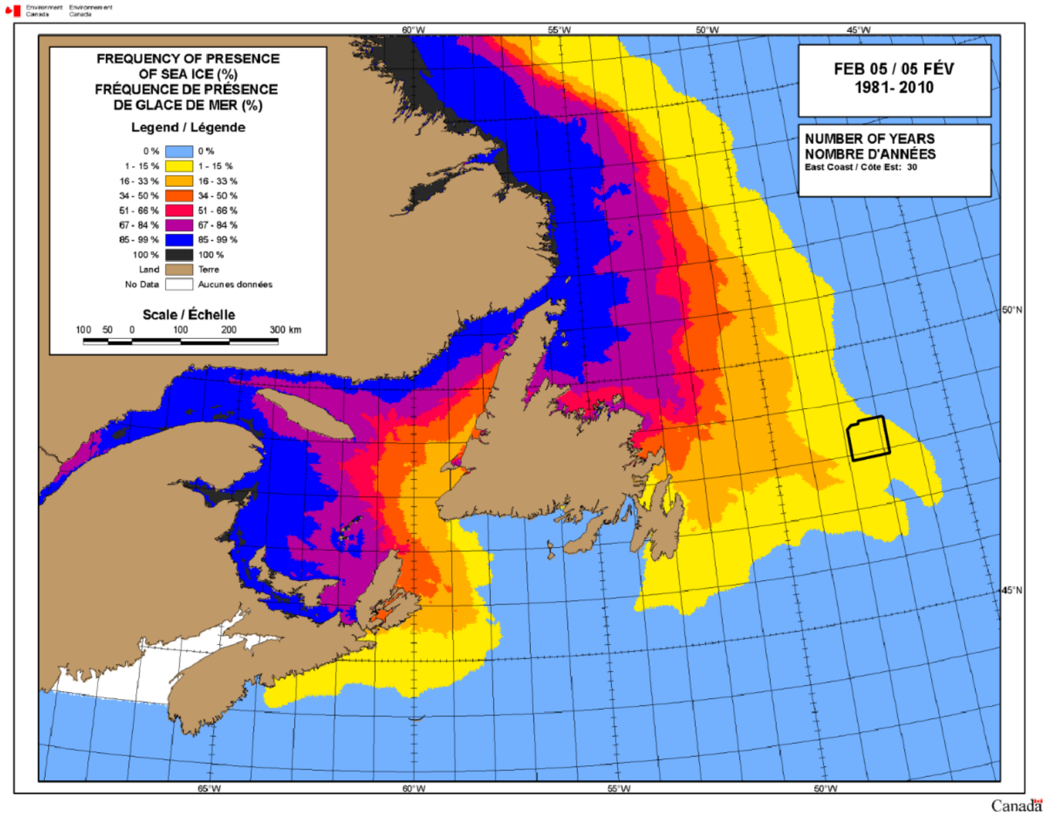

Source: Canadian Ice Service

Figure 5-26 Weekly Analysis of 30-year Frequency of Presence when Ice is Present in the Study Areas (black polygon) in the Week Starting from February 5, 1981-2010

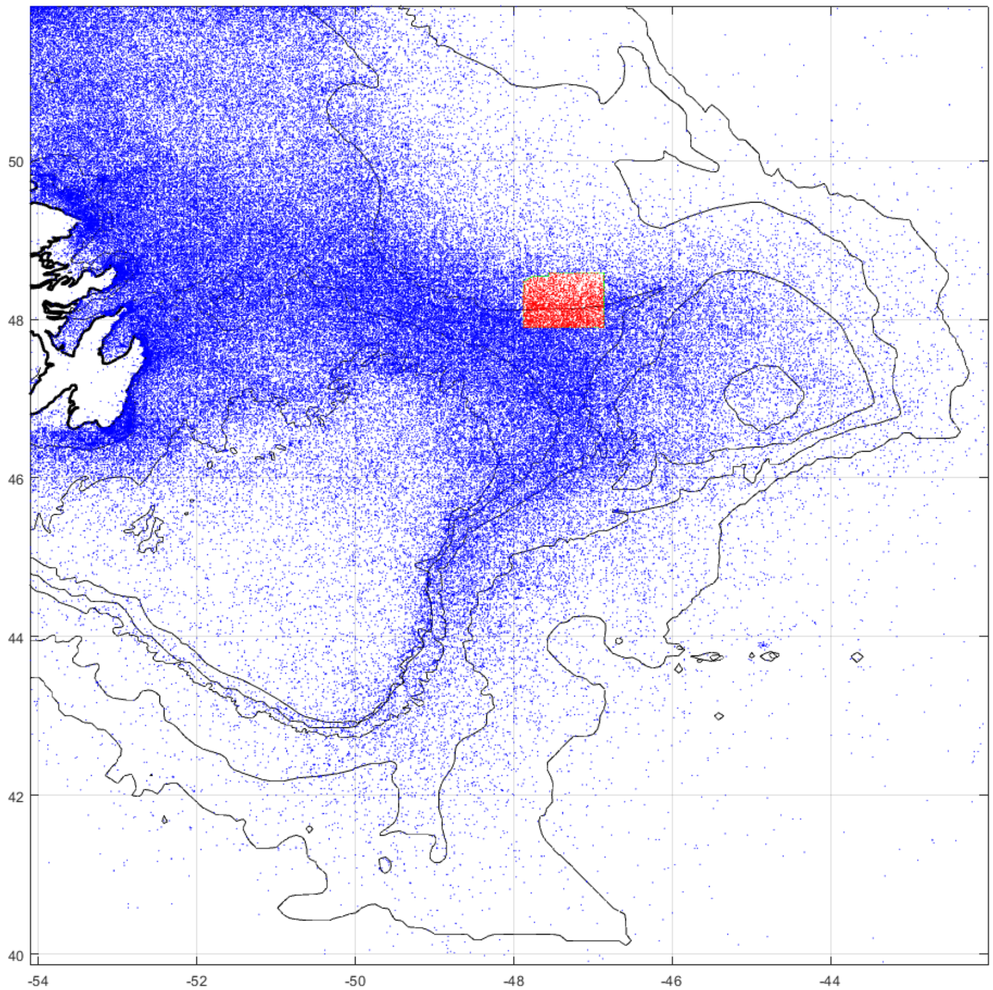

Source: International Ice Patrol 1960-2017
Project Area is highlighted in red.

Figure 5-27 Distribution of International Ice Patrol Iceberg Sightings from 1960 to 2017

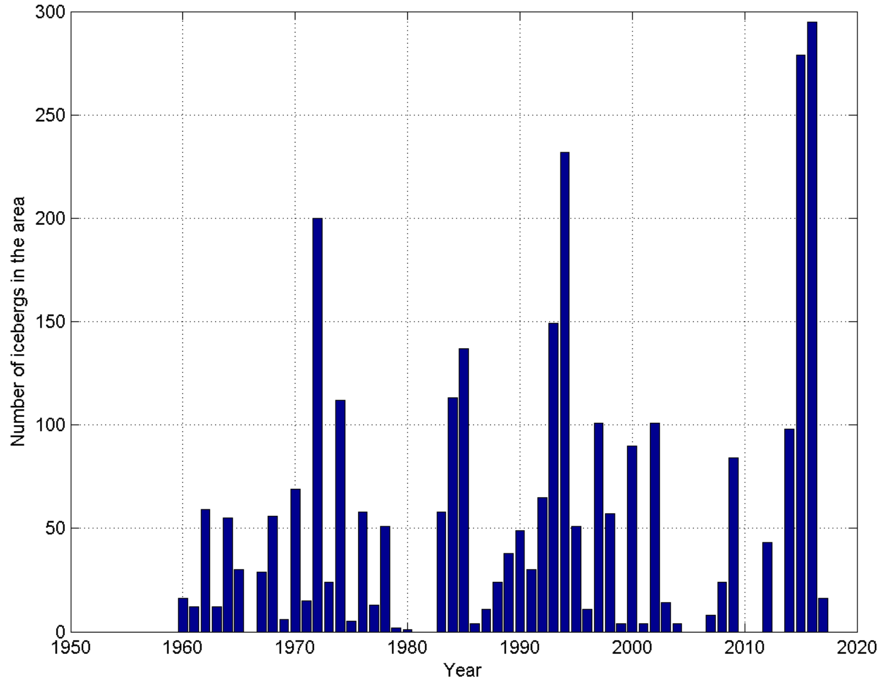

Source: International Ice Patrol 1960-2017

Figure 5-28 Iceberg Count by Years in the Research Area from 1960 to 2017

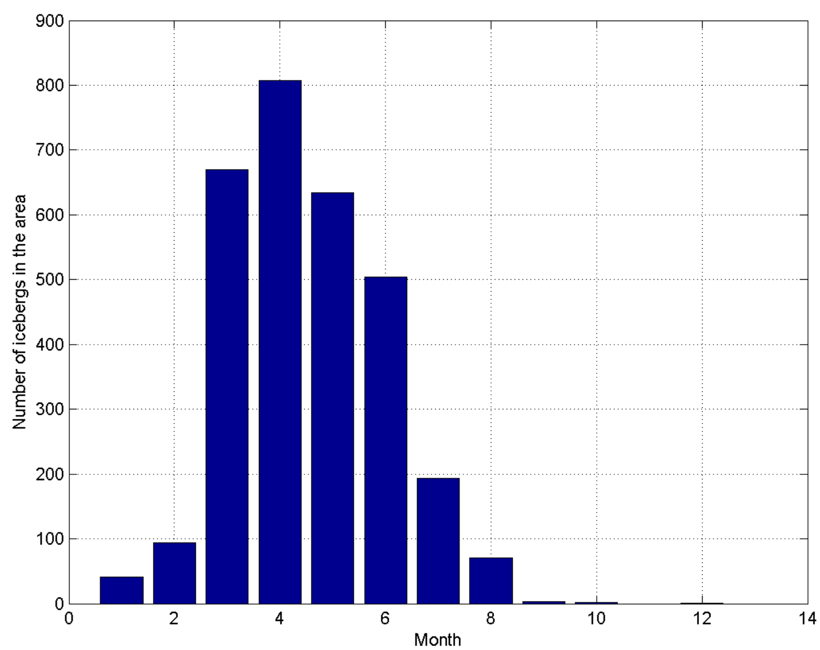

Source: International Ice Patrol 1960-2017

Figure 5-29 Iceberg Count by Month in the Research Area from 1960 to 2017

5.9.3 Marine Icing

Spray icing can accumulate on vessels and shore structures when air temperatures are below the freezing temperature of water and there is potential for spray generation. In addition to air temperature, icing severity depends on water temperature, water salinity, wave conditions, and wind speed, which influence the amount of spray and the cooling rate of droplets. Based on the algorithm (described in Appendix E; Section 4), the terminology and associated vessel icing rates for freezing spray forecasts are shown in Table 5.20. These rates and terminology are used when forecasting freezing spray on the Grand Banks.

Table 5.20 Intensity of Freezing Spray

Intensity Term	PPR	Icing Rate (cm per hour)
None	<0	0
Light	0-22.4	<0.7
Moderate	22.4-53.3	0.7-2.0
Heavy	53.3-83.0	2.0-4.0
Extreme	>83.0	>4.0

Potential icing rates are computed using wind speed, air temperature, and sea surface temperature from the ICOADS data set from 1984 to 2015. Monthly, seasonal, and annual summaries are presented in Appendix E; Table 4-1 and Figure 4-1.

Potential spray icing conditions start during the month of November with a frequency of icing potential of just 0.6%. As temperatures cool throughout the winter, the frequency of icing potential increases to a maximum of 31.5% of the time in January. Extreme sea spray icing conditions are calculated to occur 1.6% and 1.5% of the time during February and March. Icing potential decreases rapidly after March in response to warming air and sea surface temperatures, and by May the frequency of icing conditions is only 0.1%.

5.10 Climate Change

Climate change is defined as a change in the state of climate in a given region, identified by changes in the mean or variability of its properties, and persists for an extended period. Climate change can be caused by natural events, including volcanic eruptions and solar cycles, or by anthropogenic (human) activities (International Panel on Climate Change [IPCC] 2014).

GHG emissions, released from human activities and urban development, are recognized as being a contributing factor to climate change by the IPCC (2014). A GHG is any gas that contributes to potential climate change, including, but not limited to, CO_2, methane (CH_4) and nitrous oxide (N_2O). GHGs absorb and trap heat that is radiated by the earth, preventing heat from escaping to the atmosphere (ECCC 2019c). This phenomenon is commonly known as the “greenhouse effect”. An increase in GHGs in the atmosphere intensifies the GHG effect by increasingly trapping heat within the atmosphere, which in turn increases the potential for climate change and related effects. These effects include, but are not limited to, changes to temperatures, changes to meteorological patterns and intensities of precipitation and storms, and sea level rise (IPCC 2014; United States Global Change Research Program 2017).

To assess the environmental effects of climate on the Project, current climate, extreme weather, and potential climate change must be considered in the design of marine structures, so structural integrity can be maintained throughout the structure's lifetime (Vanem 2017). Current climate conditions are established by compiling relevant historical data and establishing a climatological background for the Project Area (Section 5.4). Predictions of future climate trends are derived from mathematical and statistical models.

Researchers have indicated that changes to climate will accelerate over the next century, as has been the case with temperatures around the globe over the last two decades (IPCC 2007a, 2007b). There is a consensus among the scientific community that, over the next century, Atlantic Canada is likely to experience warmer temperatures, increased precipitation, and increased storm intensity (Lines et al. 2005; Lemmen et al. 2008; Vasseur and Catto 2008).

The most relevant climate-related changes to the Project include 1) atmospheric climate change, including changes to temperature, precipitation, winds, and storms; and 2) oceanographic climate change, including changes to ocean water temperature, waves/currents, seal level, sea ice, and icebergs.

5.10.1 Atmospheric Climate Change

5.10.1.1 Temperature

Mean (average) annual air temperatures have been increasing over the last century on the East Coast of Canada, which includes Newfoundland and Labrador. Data collected between 1990 and 2010 show that average air temperatures in the East Coast region have increased by 0.90±0.37°C and stations located along the Atlantic Ocean show that average air temperatures have increased by 0.75±0.34°C (Savard et al. 2016).

Temperatures on the East Coast of Canada are projected to increase by 1.6 to 3.8°C by 2050 (Savard et al. 2016) (Table 5.21). Air temperatures during the winter season are expected to see the largest change over time. This agrees with projected increases presented in other studies (Finnis 2013; Galbraith and Larouche 2013) and global temperature increase projections (IPCC 2013).

Table 5.21 Projected Change of Near-surface Air Temperatures in the East Coast of Canada Region for 30-Year Periods

Season	Change by 2020	Change by 2050	Change by 2080
Winter	1.4 to 2.2°C	2.5 to 3.8°C	3.4 to 5.0°C
Spring	0.8 to 1.5°C	1.6 to 2.7°C	2.2 to 4.1°C
Summer	0.9 to 1.6°C	1.7 to 2.7°C	2.2 to 3.8°C
Fall	1.1 to 1.6°C	1.9 to 2.8°C	2.3 to 4.1°C
Source: Savard et al. 2016 Note: Changes are relative to data collected in 1970-2000			

The province of NL commissioned a climate change projections study in 2018, to identify how the province's temperature will change in the future compared to the 20th century. The results of the study indicate that the daily mean temperature is predicted to increase by 3.3°C on average by the 2041-2070 period (Government of NL 2018).

5.10.1.2 Precipitation

Precipitation on the East Coast of Canada is expected to increase from 0.3% to 15.4% by 2050. Future precipitation is projected to increase in the winter and spring and could decrease in the summer and fall (Savard et al. 2016) (Table 5.22).

Table 5.22 Projected Change of Precipitation in the East Coast of Canada Region for 30-Year Periods

Season	Change by 2020	Change by 2050	Change by 2080
Winter	2.8 to 9.7%	6.5 to 15.4%	12.6 to 22.9%
Spring	0.3 to 8.1%	3.1 to 11.5%	8.8 to 18.5%
Summer	–1.9 to 5.2%	–1.4 to 5.7%	–4.0 to 7.1%
Fall	–2.8 to 3.6%	–2.0 to 7.1%	–0.9 to 10.1%
Source: Savard et al. 2016 Note: Changes are relative to data collected in 1970-2000			

According to the NL climate change projections study, the daily mean precipitation is predicted to increase by 0.4 mm[1] on average by 2041-2070 (Government of NL 2018). The study also estimates the number of days within a year with 10 mm or more precipitation is expected to increase by one to four days by 2041, depending on the season and the location (Government of NL 2018).

The predicted future increases in spring and winter temperatures and precipitation (Tables 5.21 and 5.22) would suggest that the proportion of winter precipitation falling as snow is likely to decrease and rain or freezing rain would potentially increase. This is in alignment with the Finnis (2013) study of predicted impacts of climate change in NL. Wet, heavy snow and freezing rain and ice can potentially damage infrastructure and be a hazard to transportation. Historically, eastern Newfoundland has had the highest amount of freezing rain in Canada, experiencing up to 40 hours of seasonal total freezing rain hours (October to May, 1952-2007) (Cheng et al. 2011).

5.10.1.3 Wind and Storms

Determining historical trends in wind speed and direction is difficult because wind data sets are often not as complete as temperature and precipitation data sets. Wind is sensitive to topography, such as hills and valleys, and any movement of the wind monitoring stations or maintenance on the wind monitoring equipment would lead to skews in the collected data (Savard et al. 2016).

Research indicates that climate change is unlikely to result in changes in wind speed in the future; however, storm paths could shift northward which could increase storm frequency on the East Coast of Canada (Loder et al. 2013; Savard et al. 2014; Salon 2017). Historical data shows that the northwestern Atlantic Ocean, the Labrador Sea, and the Gulf of St. Lawrence are some of the stormiest areas in North America (Savard et al. 2016).

[1] When considering annual precipitation, snowfall depth equates to a liquid depth of precipitation by a factor of approximately 10 mm snow to 1 mm precipitation.

Research advises that storm frequency is likely to increase in the future (Lines et al. 2005; Lemmen et al. 2008; Vasseur and Catto 2008; Christensen et al. 2013; Collins et al. 2013). It is thought that warmer sea subsurface temperatures tend to generate longer and more intense storms (also known as tropical cyclones or hurricanes) (Ocean and Climate Platform 2019). However, there is a low confidence in future predictions of storm conditions (Church et al. 2013).

5.10.2 Oceanographic Changes

5.10.2.1 Ocean Temperature

Historically, global ocean warming has been most observed near the surface, with the upper 75 m warmed by 0.11°C each decade from 1971-2010. The IPCC predicts, with high confidence, that global ocean waters will continue to warm throughout the 21st Century and beyond (IPCC 2014).

The annual mean ocean temperature off the coast of Newfoundland and Labrador is predicted to increase in the future, based on recent climate change study results. The surface temperature of the ocean is predicted to increase by 1.4°C (±0.6°C), and the bottom ocean temperature is expected to increase by 1.6°C (±0.9°C) by 2040-2069 (Han et al. 2019).

5.10.2.2 Waves and Currents

Wave modelling is commonly used in coastal vulnerability assessments and in the planning/design of offshore infrastructure projects, such as drilling platforms, wharves, jetties, breakwaters, and offloading/loading structures (Savard et al. 2016). Changes in ocean waves are determined by changes in the major wind systems (Church et al. 2013). Wave heights have increased in the north Atlantic Ocean since the mid-1980s (Church et al. 2013). Although there have been studies conducted on future ocean wave patterns, there is a low confidence in the results (Church et al. 2013).

Ocean currents are affected by wind, temperature, and differences in salinity. Water currents flow around oceans in a conveyer-belt pattern that moves warm and cold water around the world. Ocean currents play a fundamental role in influencing climate around the world (National Oceanic and Atmospheric Administration 2018). Changes in surface winds, ocean warming, and melting ice can alter ocean currents (Church et al. 2013). Although observations of ocean circulation are fewer in comparison with ocean temperature, there is growing evidence of variability and changes of ocean current patterns related to climate change (Rhein et al. 2013). For example, the Labrador Current (the current of cold water that flows from the Arctic Ocean south along the coast of NL and along the east coast of Nova Scotia) was shown to have weakened in strength from 1992 to 2012 (Han et al. 2014).

5.10.2.3 Sea Level

From 1901 to 2010, global mean sea levels increased by 0.19 m (IPCC 2014). The rate of sea level rise has increased over the 20th century, mainly from warming of the ocean causing thermal expansion and glacier melting (Zhai et al. 2014). The IPCC has estimated that the occurrence of future sea level extreme events (which will increase with mean sea level rise) will increase substantially in the future (Church et al. 2013).

Zhai et al. (2014) predicted that sea level rise for the East Coast of Canada, for the period of 1995-2050, will be between 0.13 and 0.45 m. However, in Atlantic Canada, some land is sinking, which can produce regional differences that global climate change models do not take into consideration (Savard et al. 2016). In a recent study, sea levels are predicted to rise by 0.11 m at the St. John's, NL, tide-gauge station (between 2011 and 2069) because of changes in the ocean, such the prediction that the Labrador Current will double its freshwater transport from ice melt in the Arctic (Han et al. 2019).

5.10.3 Ice Conditions

5.10.3.1 Sea Ice

Warmer temperatures associated with climate change can decrease ice cover (i.e., area), thickness, and the duration of the ice-covered season. Changes in sea ice can have impacts on marine navigation and wind/waves reaching coastal areas (e.g., sea ice dampens wave action) (Savard et al. 2016).

The average annual sea ice cover in East Coast of Canada decreased by 1.53% per year from 1998 to 2013 (Savard et al. 2016). Sea ice melt is expected to continue, with modelling predicting that sea ice may be completely absent from most of the Gulf of St. Lawrence by 2100 (Senneville et al. 2014). The extent of winter sea ice in Newfoundland and Labrador is projected to decrease by 70% by 2069 (Han et al. 2019).

5.10.3.2 Icebergs

Icebergs are a hazard in the northwest Atlantic Ocean; there are records of collisions and ships sinking as far back as the 17th century (Marsh et al. 2018). Icebergs, as well as sea ice, can impact other activities as well; they are often monitored as part of ice management plans for offshore oil and gas exploration and development (AMEC 2011).

Han et al. (2015) estimated that warmer ocean temperatures could reduce the number of icebergs at 48°N off the coast of Newfoundland by 30% to 100% in the next 50 years.

5.11 References

AMEC (AMEC Environment & Infrastructure – A Division of AMEC Americas). 2011. A Study of Climate Monitoring Capabilities in Newfoundland and Labrador. Available at: https://www.exec.gov.nl.ca/exec/occ/publications/climate_monitoring_capabilities_nl.pdf.

Amec (Amec Environment & Infrastructure). 2014. Eastern Newfoundland and Labrador Offshore Area Strategic Environmental Assessment Update. Submitted to Canada-Newfoundland and Labrador Offshore Petroleum Board, St. John's, NL.

Bernier N. B and K. R. Thompson, 2006. Predicting the frequency of storm surges and extreme sea levels in the northwest Atlantic. J. Geophys. Res., 111: C10009, doi:10.1029/2005JC003168

Bigg, G.R. 2016. Icebergs: Their Science and Links to Global Change. Cambridge University Press, Cambridge. 250 pp.

Cameron, G.D.M. and M.A. Best. 1985. Surface Features of the Continental Margin of Eastern Canada. Map compilation for the Atlantic. Geoscience Centre, Bedford Institute of Oceanography, Beford, NS.

Cameron, G.D.M., Piper, D.J.W., and MacKillop, K. 2014. Sediment failures in northern Flemish Pass; Geological Survey of Canada, Open File 7566. Available at: http://publications.gc.ca/collections/collection_2014/rncan-nrcan/M183-2-7566-eng.pdf.

Canadian Ice Service (CIS). No Date. 30-year Climatic Ice Atlases. Available at: https://www.ec.gc.ca/glaces-ice/?lang=En&n=090AF7D6-1

CBC News. 2017. Almost 1,000 Icebergs Counted in N.L. Shipping Lanes So Far This Year. July 11, 2017. Available at: https://www.cbc.ca/news/canada/newfoundland-labrador/iceberg-alley-newfoundland-1.4199042.

Cheng, C.S., Guilong L. and H. Auld. 2011. Possible impacts of climate change on freezing rain using downscaled future climate scenarios: Updated for Eastern Canada, Atmos.-Ocean, 49:1, 8-21.

Christensen, J.H., K. Krishna Kumar, E. Aldrian, S.-I. An, I.F.A. Cavalcanti, M. de Castro, W. Dong, P. Goswami, A. Hall, J.K. Kanyanga, A. Kitoh, J. Kossin, N.-C. Lau, J. Renwick, D.B. Stephenson, S.-P. Xie and T. Zhou. 2013: Climate Phenomena and their Relevance for Future Regional Climate Change. In: Climate Change 2013: The Physical Science Basis. Contribution of Working Group I to the Fifth Assessment Report of the Intergovernmental Panel on Climate Change. Available at: https://www.ipcc.ch/report/ar5/wg1/.

Church, J.A., P.U. Clark, A. Cazenave, J.M. Gregory, S. Jevrejeva, A. Levermann, M.A. Merrifield, G.A. Milne, R.S. Nerem, P.D. Nunn, A.J. Payne, W.T. Pfeffer, D. Stammer and A.S. Unnikrishnan.2013. Sea Level Change. In: Climate Change 2013: The Physical Science Basis. Contribution of Working Group I to the Fifth Assessment Report of the Intergovernmental Panel on Climate Change. Available at: https://www.ipcc.ch/report/ar5/wg1/.

Collins, M., R. Knutti, J. Arblaster, J.-L. Dufresne, T. Fichefet, P. Friedlingstein, X. Gao, W.J. Gutowski, T. Johns, G. Krinner, M. Shongwe, C. Tebaldi, A.J. Weaver and M. Wehner. 2013. Long-term Climate Change: Projections, Commitments and Irreversibility. In: Climate Change 2013: The Physical Science Basis. Contribution of Working Group I to the Fifth Assessment Report of the Intergovernmental Panel on Climate Change. Available at: https://www.ipcc.ch/report/ar5/wg1/.

Delarue, J., K.A. Kowarski, E.E. Maxner, J.T. MacDonnell and S.B. Martin. 2018. Acoustic Monitoring Along Canada's East Coast: August 2015 to July 2017. Document Number 01279, Environmental Studies Research Fund Report Number 215, Version 1.0. Technical report by JASCO Applied Sciences for Environmental Studies Research Fund, Dartmouth, NS. 120 pp + Appendices.

Dragoset, W.H. 1984. A comprehensive method for evaluating the design of airguns and airgun arrays. PP. 75-84. In: Proceedings, 16th Annual Offshore Technology Conference Volume 3, 7-9 May 1984. OTC 4747, Houston, TX.

ECCC (Environment and Climate Change Canada). 2016. Lightning Activity in Canadian cities. Available at: https://www.canada.ca/en/environment-climate-change/services/lightning/statistics/activity-canadian-cities.html

ECCC (Environment and Climate Change Canada). 2019a. NPRI Data Search. Available at: https://pollution-waste.canada.ca/national-release-inventory/archives/index.cfm?do=query&lang=en

ECCC (Environment and Climate Change Canada). 2019b. Greenhouse Gas Reporting Program. Available at: https://climate-change.canada.ca/facility-emissions/?GoCTemplateCulture=en-CA

ECCC (Environment and Climate Change Canada). 2019c. Canadian Environmental Sustainability Indicators. Greenhouse Gas Emissions. Available at: https://www.canada.ca/content/dam/eccc/documents/pdf/cesindicators/ghg-emissions/2019/national-GHG-emissions-en.pdf.

Edinger, E.N., O.A. Sherwood, D.J.W. Piper, V.E. Wareham, K.D. Baker, K.D. Gilkinson and D.B. Scott. 2011. Geological features supporting deep-sea coral habitat in Atlantic Canada. Continental Shelf Research, 31: 569-584.

Edwards, T., Jauer, C.D., Moir, P., and Wielens, J.B.W. (Eds.) 2003. Tectonic Elements, Grand Banks of Newfoundland (East Coast Basin Atlas Series). Geological Survey of Canada, Open File 1795. Available at: http://ftp.maps.canada.ca/pub/nrcan_rncan/publications/ess_sst/214/214599/of_1795.pdf.

Enachescu, M. 2006. Structural Setting and Petroleum Potential of the Orphan Basin, offshore Newfoundland and Labrador. CSEG Recorder, 31(2). Available at: https://csegrecorder.com/articles/view/structural-setting-and-petroleum-potential-of-orphan-basin-offshore-nfld.

Enachescu, M.E. 2011. Petroleum Exploration Opportunities in Area "C" - Flemish Pass/North Central Ridge Call for Bids NL11-02. Prepared for Government of Newfoundland and Labrador Department of Natural Resources. Available at: http://www.nr.gov.nl.ca/nr/invest/enachescu_NL1102Flemish.pdf.

Enachescu, M. 2012a. Call for Bids NL12-02, Parcel 1, Petroleum Exploration Opportunities in the Flemish Pass Basin. Government of Newfoundland and Labrador Department of Natural Resources. Available at: https://www.nr.gov.nl.ca/nr/invest/call_bids_petro_exploration_enachescu%20.pdf.

Enachescu, M. 2012b. Offshore Opportunity – 2012 Licence Round. Call for Bids NL12-02, Flemish Pass Basin, Offshore Newfoundland. Government of Newfoundland and Labrador Department of Natural Resources. Available at: https://www.nr.gov.nl.ca/nr/invest/NL1202Sum.pdf.

Enachescu, M. 2014a. Petroleum Exploration Opportunities in the Flemish Pass Basin, Newfoundland and Labrador Offshore Area: Call for Bids NL13-01, Area "C" – Flemish Basin, Parcel 1. Prepared for Government of Newfoundland Department of Natural Resources. Available at: https://www.nr.gov.nl.ca/nr/invest/NL1301FlemishPassBasinEnachescu.pdf.

Enachescu, M. 2014b. Offshore Opportunity – 2013 Licence Round. Call for Bids NL13-01, Flemish Pass Basin, Offshore Newfoundland. Government of Newfoundland and Labrador Department of Natural Resources. Available at: https://www.nr.gov.nl.ca/nr/invest/FlemishPassFolio.pdf.

Enachescu, M. and Fagan, P. 2004. Newfoundland and Labrador Call for Bids NF04-01, Government of Newfoundland and Labrador, Department of Natural Resources. 35p, 20 figures. Available at: http://www.nr.gov.nl.ca/nr/invest/cfb_nl04_01_jab.pdf.

Enachescu, M., S. Kearsey, V. Hardy, J.-C. Sibuet, J. Hogg, S.P. Srivastava, A. Fagan, T. Thompson and R. Ferguson. 2005. Evolution and Petroleum Potential of Orphan Basin, Offshore Newfoundland, and Its Relation to the Movement and Rotation of Flemish Cap based on Plate Kinematics of the North Atlantic. Gulf Coast Section Society for Sedimentary Geology, Pp: 75-131. Conference Paper: Petroleum Systems of Divergent Continental Margin Basins, 25th Annual GCSSEPM Foundation - Bob F. Perkins Research Conference, Houston, TX. DOI: 10.5724/gcs.05.25.0075.

Equinor (Equinor Canada Ltd.) 2018. Bay du Nord Development Project – Project Description. Available at: https://www.cnlopb.ca/wp-content/uploads/equinor/projdesc.pdf.

ExxonMobil Canada Properties. 2011. Hebron Project Comprehensive Study Report. Submitted to the Canada-Newfoundland and Labrador Offshore Petroleum Board, St. John's, NL. Available at: https://www.cnlopb.ca/assessments/hebron/

Fader, G.B., G.D.M. Cameron and M.A. Best. 1989. Geology of the Continental Margin of Eastern Canada, Geological Survey of Canada. Map 1705A.

Finnis, J. 2013. Projected Impacts of Climate Change for the Province of Newfoundland and Labrador; Report Prepared for the Office of Climate Change. Available at: http://turnbackthetide.ca/whatsnew/2013/NL_Climate_Projections_Full_Report.pdf.

G and G Exploration Consulting Ltd. 2003. Hydrocarbon Potential of Parcels 1-12, C-NOPB Call for Bids NF 03-1. Orphan Basin Offshore Newfoundland. Canadian Journal of Earth Sciences, 22: 504-526.

Galbraith, P.S. and Larouche, P. 2013. Trends and variability in air and sea surface temperatures in eastern Canada; in Aspects of Climate Change in the Northwest Atlantic off Canada, (ed.) J.W. Loder, G. Han, P.S. Galbraith, J. Chassé, and A. van der Baaren; Fisheries and Oceans Canada, Ottawa, ON. Canadian Technical Report of Fisheries and Aquatic Sciences, 3045: 1-18. Available at: http://publications.gc.ca/collections/collection_2014/mpo-dfo/ Fs97-6-3045-eng.pdf.

Government of NL (Newfoundland and Labrador). 2018. Projected Impacts of Climate Change for the Province of Newfoundland and Labrador. 2018 Update. Available at: https://www.turnbackthetide.ca/tools-and-resources/whatsnew/2018/Final_Report_2018.pdf Excel spreadsheets available at: https://www.exec.gov.nl.ca/exec/occ/climate-data/index.html.

Han, G., N. Chen and Z. Ma. 2014. Is There a North-south Phase Shift in the Surface Labrador Current on the Interannual-todecadal Scale, J. Geophys. Res. Oceans, 119: 276-287.

Han, G., E. Colbourne, P. Pepin and Y. Xie. 2015. Statistical Projections of Ocean Climate Indices off Newfoundland and Labrador. Atmos.-Ocean, 53(5): 556-570.

Han, G. and J. Li., 2004. Sea Surface Height and Current Variability on the Newfoundland Slope from TOPEX/Poseidon Altimetry. Can. Tech. Rep. Hydrogr. Ocean Sci., 234: 40 pp.

Han, G., Z. Ma, Z. Long, W. Perrie and J. Chasse. 2019. Climate Change on Newfoundland and Labrador Shelves: Results from a Regional Downscaled Ocean and Sea-Ice Model Under a A1B Forcing Scenario 2011-2069. Atmos.-Ocean, 57:1, 3-17.

Han, G., and C.L. Tang, 1999. Velocity and transport of the Labrador Current determined from altimetric, hydrographic and wind data, J. Geophys. Res., 104: 18047-18057.

International Ice Patrol. 1960-2017. International Ice Patrol Iceberg Sightings Database Updated through 2017. Available at: https://nsidc.org/the-drift/data-update/international-ice-patrol-iceberg-sightings-database-updated-through-2017/

IPCC (Intergovernmental Panel on Climate Change). 2007a. Climate Change 2007a: The Physical Science Basis, Summary for Policymakers. Contribution of Working Group I to the Fourth Assessment Report of the Intergovernmental Panel on Climate Change, IPCC Secretariat, Geneva, 21 pp. Available at: https://www.ipcc.ch/pdf/assessment-report/ar4/wg1/ar4-wg1-spm.pdf

IPCC (Intergovernmental Panel on Climate Change). 2007b. Appendix I: Glossary. Pp. 869-883. In: M.I. Parry, O.F. Canziani, J.P. Palutidof, P.J. van der Linden and C.E. Hanson (eds.). Climate Change 2007: Impacts, Adaptation and Vulnerability (Contribution of Working Group II to the Fourth Assessment Report of the Intergovernmental Panel on Climate Change), Cambridge University Press, Cambridge United Kingdom. Available at: http://www.ipcc.ch/pdf/assessment-report/ar4/wg2/ar4-wg2-app.pdf.

IPCC (Intergovernmental Panel on Climate Change). 2013. Summary for policymakers; in Climate Change 2013: The Physical Science Basis (Contribution of Working Group I to the Fifth Assessment Report of the Intergovernmental Panel on Climate Change), (ed.) T.F. Stocker, D. Qin, G.-K. Plattner, M. Tignor, S.K. Allen, J. Boschung, A. Nauels, Y. Xia, V. Bex and P.M. Midgley; Cambridge University Press, Cambridge, United Kingdom and New York, New York, 27 pp. Available at: http://www.ipcc.ch/pdf/ assessment-report/ar5/wg1/WGIAR5_SPM_brochure_en.pdf.

IPCC (International Panel on Climate Change). 2014. Climate Change 2014. Synthesis Report. Contribution of Working Groups I, II and III to the Fifth Assessment Report of the Intergovernmental Panel on Climate Change. Available at: https://archive.ipcc.ch/pdf/assessment-report/ar5/syr/SYR_AR5_FINAL_full_wcover.pdf.

Kennard, L., C. Schaefer and L. Carter. 1990. Late Cenozoic evolution of Sackville Spur: a sediment drift on the Newfoundland continental slope. Canadian Journal of Earth Sciences, 27: 865-878.

King, L.H., G.B.J. Fader, W.H. Poole and R.K. Wanless. 1985. Geological setting and age of the Flemish Cap granodiorite, east of the Grand Banks of Newfoundland. Canadian Journal of Earth Sciences, 22: 1286-1298.

King, L.H., G.B.J. Fader, W.A.M. Jenkins and E.L. King. 1986. Occurrence and regional geological setting of Paleozoic rocks on the Grand Banks of Newfoundland. Canadian Journal of Earth Sciences, 23(4): 504-526.

Lazier, J.R.N. and D.G. Wright 1993. Annual Velocity variations in the Labrador Current, J. Phys. Oceanogr., 23, p.659-678.

Lemmen, D.S., F.J. Warren, J. Lacroix and E. Bush. 2008. From Impacts to Adaptation: Canada in a Changing Climate 2007. Government of Canada, Ottawa, ON, 448 pp. Available at: https://www.nrcan.gc.ca/environment/resources/publications/impacts-adaptation/reports/assessments/2008/10253.

Lines, G.S., M. Pancura and C. Lander. 2005. Building Climate Change Scenarios of Temperature and Precipitation in Atlantic Canada using the Statistical Downscaling Model (SDSM). Environment Canada, Meteorological Service of Canada, Atlantic Region. Available at: https://climatechange.novascotia.ca/sites/default/files/uploads/Building_Climate_Scenarios.pdf.

Loder, J.W., G. Han, P.S. Galbraith, J. Chassé and A. van der Baaren. 2013. Aspects of Climate Change in the Northwest Atlantic off Canada; Fisheries and Oceans Canada, Dartmouth, Nova Scotia, Canadian Technical Report of Fisheries and Aquatic Sciences, 3045: 190 pp.

Lowe, D.G., P.J. Sylvester and M.E. Enachescu. 2011. Provenance and paleodrainage patterns of upper Jurassic and Lower Cretaceous synrift sandstones in the Flemish Pass Basin, offshore Newfoundland, east coast of Canada. AAPG Bulletin, 95: 1295-1320.

Marsh, R., G. Bigg, Y. Zhao, Y. M.J. Martin, J.R. Blundell, S.A. Josey, E. Hanna and V. Ivchenko. 2018. Prospects for seasonal forecasting of iceberg distributions in the North Atlantic. Natural Hazards, 91(2): 447-471.

Marshall, N.R., D.J.W. Piper, F. Saint-Ange and D.C. Campbell. 2014. Late Quaternary history of contourite drifts and variations in Labrador Current flow, Flemish Pass, offshore eastern Canada. Geo-Marine Letters, 34(5): 457-470.

Matthews, M-N, T.J. Deveau, C. Whitt and B. Martin. 2018. Underwater Sound Assessment for Newfoundland Orphan Basin Exploration Drilling Program. Document 01592, Version 4.0. Technical report by JASCO Applied Sciences for Stantec.

Murillo, F.J., Kenchington, E., Lawson, J.M., Li, G., and Piper, D.J.W. 2016. Ancient deep-sea sponge grounds on the Flemish Cap and grand Bank, northwest Atlantic. Marine Biology, 163 (3): 63 (11 pp.).

National Oceanic and Atmospheric Administration. 2018. Ocean Explorer. Available at: https://oceanexplorer.noaa.gov/facts/climate.html.

NRCan (Natural Resources Canada). 2018. Seismic Hazard Map # 10 (of 11): 201 National Building Code of Canada Available at: http://earthquakescanada.nrcan.gc.ca/hazard-alea/zoning-zonage/images/GSC2015PGApdf.pdf

NRCan (Natural Resources Canada). 2019. Search of the Earthquakes Canada Database. Available at: http://www.earthquakescanada.nrcan.gc.ca/stndon/NEDB-BNDS/bulletin-en.php

Ocean and Climate Platform. 2019. Cyclones and Climate Change. Available at: https://ocean-climate.org/?p=4832&lang=en.

Petrie B., K. Lank, and S. de Margerie, 1987. Tides on the Newfoundland Grand Banks. Atmos.-Ocean, 25(1): 10-21.

Piper, D.J.W, A.W.A. MacDonald, S. Ingram, G.L. Williams and C. McCall. 2005. Late Cenzoic architecture of the St. Pierre Slope. Can. J. Earth Sci., 42: 1987-2000.

Rhein, M., S.R. Rintoul, S. Aoki, E. Campos, D. Chambers, R.A. Feely, S. Gulev, G.C. Johnson, S.A. Josey, A. Kostianoy, C. Mauritzen, D. Roemmich, L.D. Talley and F. Wang. 2013. Observations: Ocean. In: Climate Change 2013: The Physical Science Basis. Contribution of Working Group I to the Fifth Assessment Report of the Intergovernmental Panel on Climate Change. Available at: https://www.ipcc.ch/report/ar5/wg1/. Last accessed: June 27, 2019.

Ruffman, A.R. 2011. Orphan Knoll as a Window on the Paleozoic: Seemingly Ignored by the Petroleum Industry for Over 40 Years. 2011 CSPG CSEG CWLS Convention. 5 pp.

Salon, F, T. Tamarin, I. Rehovot and Y. Kaspi. 2017.The Poleward Shift of Storm Tracks Under Climate Change: A Lagrangian Perspective. Available at: https://ams.confex.com/ams/21Fluid19Middle/webprogram/Paper319195.html.

Savard, J.-P., P. Gachon, C. Rosu, R. Aider, P. Martin and C. Saad. 2014. Impact des changements climatiques sur le régime des tempêtes, les niveaux d'eau et les vagues dans le Nunavik; ministère des Transports du Québec, Québec, Quebec, 109 pp. Available at: http://www.ouranos.ca/media/publication/357_RapportSavard2014.pdf.

Savard, J.-P., D. van Proosdij and S. O'Carroll. 2016. Perspectives on Canada's East Coast region. Pp. 99-152. In: D.S. Lemmen, F.J. Warren, T.S. James and C.S.L. Mercer Clarke (eds.). Canada's Marine Coasts in a Changing Climate, Government of Canada, Ottawa, ON. Available at: http://www.nrcan.gc.ca/sites/www.nrcan.gc.ca/files/earthsciences/files/pdf/NRCAN_fullBook%20%20accessible.pdf.

Schrag, D.P., J.A. Higgins, F.A. MacDonald. and D.T. Johnson. 2013. Authigenic carbonate and the history of the global carbon cycle. Science, 339(6119): 540-543.

Seaconsult Ltd. 1998. Physical Environmental Data for Production Systems at Terra Nova. Report prepared for Petro-Canada Inc.

Senneville, S., S. St-Onge, D. Dumont, M.-C. Bihan-Poudec, Z. Belemaalem, M. Corriveau, P. Bernatchez, S. Bélanger, S. Tolszczuk-Leclerc and R. Villeneuve. 2014. Rapport final Modélisation des glaces dans l'estuaire et le golfe du Saint-Laurent dans la perspective des changements climatiques. In: J.-P. Savard, D. van Proosdij and S. O'Carroll (Editors). 2016. Perspectives on Canada's East Coast region. Pp. 99-152. Chapter 4. In D.S. Lemmen, F.J. Warren, T.S. James and C.S.L. Mercer Clarke (eds.). Canada's Marine Coasts in a Changing Climate, Government of Canada, Ottawa, ON. Available at: http://www.nrcan.gc.ca/sites/www.nrcan.gc.ca/files/earthsciences/files/pdf/NRCAN_fullBook%20%20accessible.pdf.

Statoil (Statoil Canada Ltd.) 2017. Flemish Pass Exploration Drilling Program – Environmental Impact Statement. Prepared by Amec Foster Wheeler and Stantec Consulting. St. John's, NL Canada. November 2017.

United States Global Change Research Program. 2017. Climate Science Special Report: Fourth National Climate Assessment, Volume I. U.S. Global Change Research Program, Washington, DC. 470 pp.

United States Geological Survey, Conservation Division, 1979. OCS Platform Verification Program. Reston, Virginia.

Vanem, E. 2017. A regional extreme value analysis of ocean waves in a changing climate. Ocean Engineering, 144(1): 277-295.

Vasseur, L. and N. Catto. 2008. Atlantic Canada. Pp. 119-170. In: D.S. Lemmen, F.J. Warren, J. Lacroix and E. Bush (eds.). From Impacts to Adaptation: Canada in a Changing Climate 2007, Government of Canada, Ottawa, ON. 448 pp. Available at: https://www.nrcan.gc.ca/sites/www.nrcan.gc.ca/files/earthsciences/pdf/assess/2007/pdf/full-complet_e.pdf.

Weitzman, J., S. Ledger, C.D. Stacey, G. Strathdee, D.J.W. Piper, K.A. Jarret and J. Higgins. 2014. Logs of short push cores, deep-water margin of Flemish Cap and the eastern Grand Banks of Newfoundland. Geological Survey of Canada, Open File 7148. 389 pp.

Williams, H., S.A. Dehler, A.C. Grant and G.N. Oakey. 1999. Tectonics of Atlantic Canada. Geoscience Canada, 26: 51-70.

Zhai L., B. Greenan, J. Hunter, T.S. James, G. Han, R. Thomson, and P. MacAulay. 2014. Estimating Sea-level Allowances for the coasts of Canada and the adjacent United States using the Fifth Assessment Report of the IPCC. Can. Tech. Rep. Hydrogr. Ocean. Sci., 300: v + 146 pp.

Zykov, M.M. and Z. Alavizadeh. 2019. Underwater Sound Associated with Exploration Drilling Offshore Eastern Newfoundland: Chevron's West Flemish Pass project. Document 01784, Version 1.1. Technical report by JASCO Applied Sciences for Stantec Consulting Ltd.